Spring 2024

Multifunctional Nanomaterial Analysis Using Inexpensive Techniques

Casey Jordan , '24

E90 Project Report

Spring 2024

Multifunctional Nanomaterial Analysis Using Inexpensive Techniques

Casey Jordan

Co-advised by Professor Everbach and Professor Riley

Table of Contents

Abstract

Designing methods to comprehensively understand nanomaterial interactions is of paramount importance as nanomaterials gain widespread use and their environmental impact becomes a concern. While current characterization methods are suitable for initial assessments, there is a need for comprehensive techniques to evaluate end-of-use scenarios and environmental effects. This report emphasizes the potential of electrochemistry as a versatile measurement tool for nanomaterial analysis. Two projects are presented, showcasing innovative analytical architectures to overcome the limitations of existing techniques. Project 1 integrates linear sweep stripping voltammetry (LSSV) and particle impact voltammetry (PIV) to achieve kinetic resolution and size analysis of silver nanoparticles (AgNPs) and silver ions (A(I)) released from nano-enabled textiles. Project 2 focuses on understanding the interaction between released AgNPs and proteins using PIV, with promising preliminary results. The integration of electrochemical methods provides a valuable toolset for achieving a balance between material innovation and environmental consciousness. This report highlights the significance of assessing nanomaterial interactions and illustrates the potential of electrochemistry in advancing nanomaterial research.

Introduction

Recently, there has been a notable increase in the use of engineered nanomaterials (ENMs). In many fields that heavily rely on ENMs today, the embedded nanoparticles in their structural matrix offer a wide range of unique properties. Silver nanoparticles (AgNPs) are particularly prevalent in the consumer industry due to their ability to dissociate into silver ions (Ag(I)), which possess antimicrobial properties against small bacteria and microorganisms[1].

While extensive research has been conducted on the development of these ENMs, methods for quantifying and understanding the release and fate of these nanomaterials are still relatively underdeveloped. Many techniques used to measure and analyze nanoparticles, in general, are expensive and require substantial sample preparation to obtain meaningful data.

Typically, laboratories utilize a combination of electron microscopy and atomic/molecular spectroscopy to measure concentrations of ionic silver and nanoparticle silver[2–4]. Although microscopy and spectroscopy are commonly employed for ENM characterization and in-situ measurement, they lack specificity and necessitate extensive sample preparation and homogeneous materials. If research aims to explore the response of these materials to external pressures such as sweat, movement, or protein binding, it is crucial to have cost-effective and highly repeatable methods for quantifying both the released ion and nanoparticle concentrations in situ.

Nanomaterial Background

In chemistry, we define a nanomaterial as any conglomeration of atoms that has at least one dimension between 1 and 100 nm[5]. For reference, a single carbon atom has an atomic radius of approximately 70-80 pm (0.07-0.08 nm). This means that, while nanoparticles are still extremely small and not visible to the human eye, they are still many orders of magnitude greater than atoms in terms of surface area and volume. Nanoparticles can come in many different shapes and surface topologies. The most common topologies are nanospheres and nanorods. Pictured in Figure 1 is a scanning electron microscope image of

copper nanospheres, nanorods, and a few other topologies (e.g., nanoprisms, nanotetrahedrals, and nanocubes).[6]

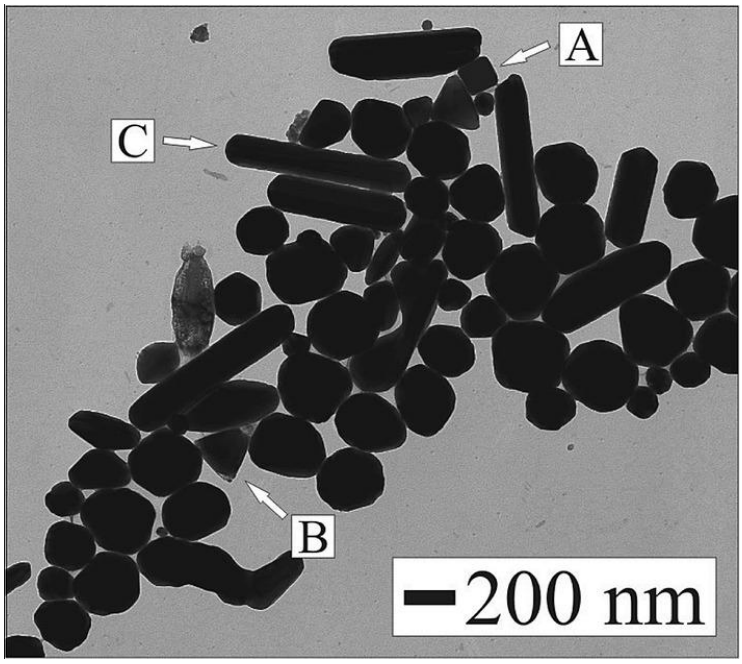

Figure 1. Scanning electron microscopy image of a mix of copper nanospheres and nanorods. Reprinted (adapted) with permission from Langmuir 2007, 23, 10, 5740–5745. Copyright 2007 American Chemical Society.

Due to these varying shapes and dimensions, nanoparticles often exhibit unique properties that differ from their bulk counterparts. As will be discussed in the following sections, the confined nature of nanoparticles leads to characteristic electrical[7], magnetic[8], and optical[9] properties which can subsequently be probed via various analytical methods. The precise tunability of ENMs, in general, has yielded many applications in a wide range of fields. ENMs are utilized in medicine for targeted drug delivery[10], in technological applications like televisions[11] and solar cells[12], and in cosmetic/commercial applications like sunscreens[13] and athletic wear[4].

Although the birth of specifically engineered nanomaterials is a relatively new addition to the material engineer's toolkit, the applications of nanomaterials and colloids in the arts and sciences have existed for millennia. The most famous example is the Lycurgus cup shown in Figure 2.

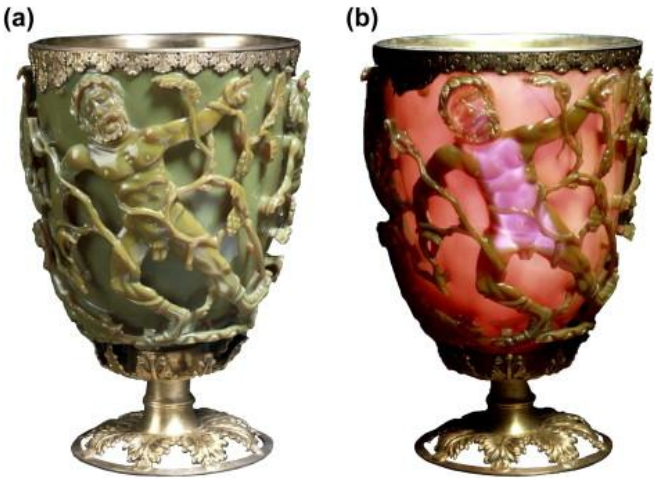

Figure 2. Image of the Lycurgus cup, a famous cup made during the 4th century AD that is painted with gold nanoparticles. When illuminated from (a) the front, it appears green and from (b) the inside, it glows red due to the nanoparticles. [From Carbon Nanotube Reinforced Composites, CNR Polymer Science and Technology, 2015, Pages 1-36, with permission]

This chalice, depicting King Lycurgus being pulled into the underworld, was made in 4th century Rome and utilized a paint containing gold nanoparticles. This caused the surface of the cup to glow red when illuminated from the inside[14]. Similar examples to this show up all over the ancient world in paintings, stained glass, and pottery.

Localized Phenomena

Nanoparticles, and more broadly ENMs as a whole, are unique in the landscape of material science and engineering as their properties are more akin to the interactions of a single particle rather than their bulk sample counterparts. This means that many of the physical properties that govern the unique characteristics of nanomaterials are due to localized phenomena on a single particle. Without diving too deep into the quantum mechanics of confined electrons and quantum tunneling, the nature of these physical phenomena can be elegantly described using a basic geometric understanding of the nanoparticle. In the following sections, the physical understanding of localized plasmonics and the unique surface properties of small ENMs will be discussed.

Localized Plasmonics

Before delving into the theory behind plasmonics, it is important to reach a baseline understanding of how light interacts with its environment. Light, or photons, move through space as oscillating waves with specific wavelengths and thus specific energies as governed by the Planck-Einstein relation in Equation 1, where h is the Planck constant, c is the speed of light, and E and λ are energy and wavelength, respectively.

$$E = \frac{hc}{\lambda} \tag{1}$$

Often, it is useful to think of each photon as a small package of energy. The faster the wave (photon) oscillates, the more energy is carried by that light. The oscillating nature of these photons creates a localized electric field that can interact with solid matter. In the case of nanoparticles, this electric field can work to oscillate the electrons bound through metallic bonds in the nanoparticle itself. This inherent delocalization of electrons from the nanoparticle surface is called surface plasmon resonance (SPR) and the fact that the resonance is confined to the surface area of a nanoparticle makes the SPR localized (LSPR)[15]. This phenomenon is demonstrated in Figure 3 for a nanosphere.

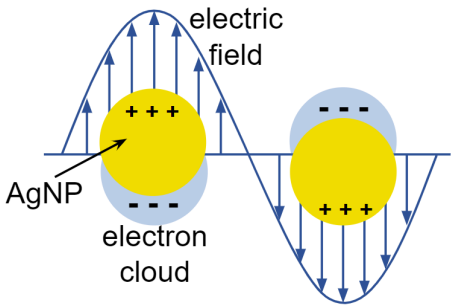

Figure 3. Demonstration of the localized surface plasmon resonance (LSPR) of a nanosphere.

The ultimate effect of this LSPR is that the nanoparticle can absorb some of the photon's energy through the oscillation of these electrons. Further, the wavelengths these nanoparticles can absorb are determined by their surface topology. Thus, a change in the surface topology of a nanoparticle can be understood by analyzing the change in the LSPR

absorbance. This is the standard method for measuring protein adsorption onto the surface of a nanoparticle.

Localized plasmonics are not only observed for zero-dimensional nanomaterials (nanospheres), however. They arise when the electrons in individual particles are confined to a small volume. This has allowed for complex analyses of nanomaterials of different shapes and sizes to be understood via various forms of resonance spectroscopy[16]. Another common form of nanomaterials that can be understood via plasmonics are nanorods (see schematic in Figure 4).

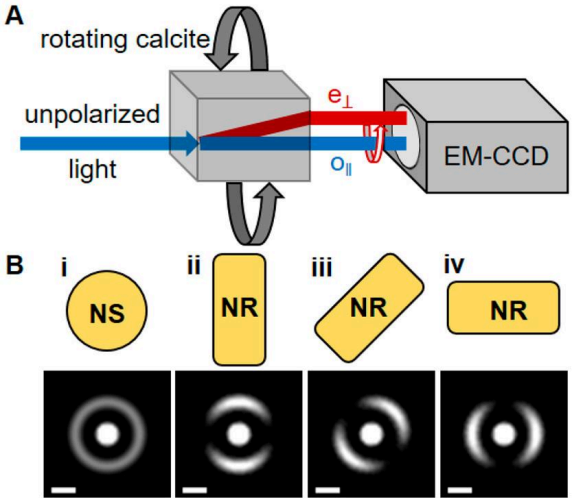

Figure 4. Schematic of calcite-assisted localization and kinetics microscopy on a series of differently oriented nanorods. Reprinted (adapted) with permission from J. Phys. Chem. Lett. 2022, 13, 45, 10527–10533. Copyright 2022 American Chemical Society.

A group at Temple has been working on a specialized technique that allows for the orientation and aspect ratio (ratio between long and short rod dimensions) of nanorods to be analyzed[17]. In that work, they utilize polarized light to specifically probe one of the axes at a time to measure the unique plasmonic resonance of each dimension separately. A schematic of this technique is shown in Figure 4.

Importantly, the light absorption intensity is greatest along the long axis of the nanorod, representing the strongest LSPR band. Here, they used a rotating calcite crystal to change the orientation of the polarized light ($e_{\perp}$).

Surface Chemistry

In addition to their photonic interactions, nanoparticles also yield a wide range of surface phenomena due to their high surface area-to-volume ratios. In general, the ratio of atoms at the surface of a particle to the total atoms in the particle increases as the size of the particles decreases as described in Figure 5.

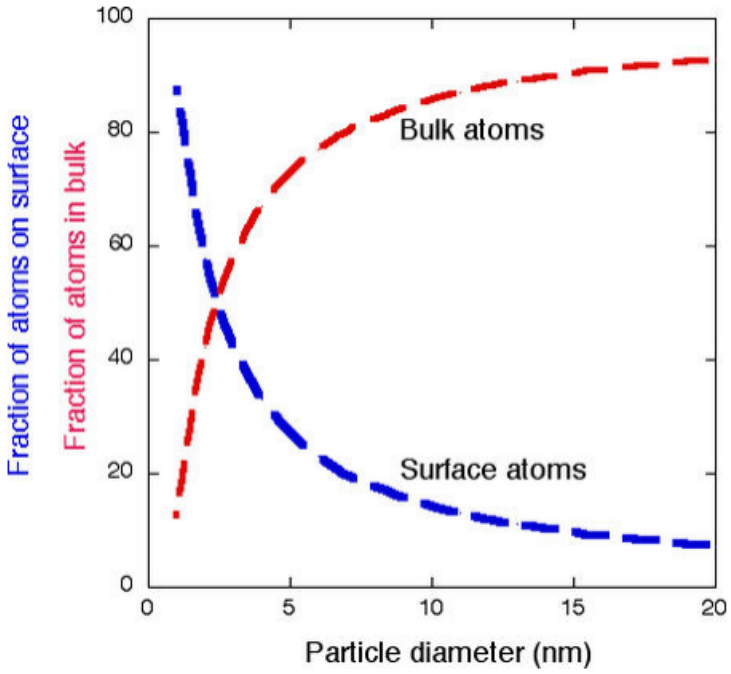

Figure 5. Fraction of particles in the bulk (red) and at the surface (blue) of a nanoparticle as a function of particle diameter.

For a perfect nanosphere, the surface area-to-volume ratio can be calculated to be:

$$\frac{SA}{V} = \frac{4\pi r^2}{\frac{4}{3}\pi r^3} = \frac{3}{r} \qquad (2)$$

This ratio is inversely proportional to the radius of the nanosphere and thus, the smaller the particle, the higher the surface area-to-volume ratio will be. However, to fully understand the phenomena that occur at the surface of nanoparticles, it is important to first discuss the notion of surface energy and how the surface area-to-volume ratio impacts surface reactivity.

Surface energy is a concept that governs a lot of different phenomena including surface tension, phase separations, and protein folding. Essentially, the idea of surface energy is that molecules on the surface of a system (e.g., water beads, nanoparticles, folded protein) undergo less stabilizing interactions with their neighboring molecules (Figure 6). This causes surface molecules to be sufficiently higher in energy than molecules trapped inside the system.

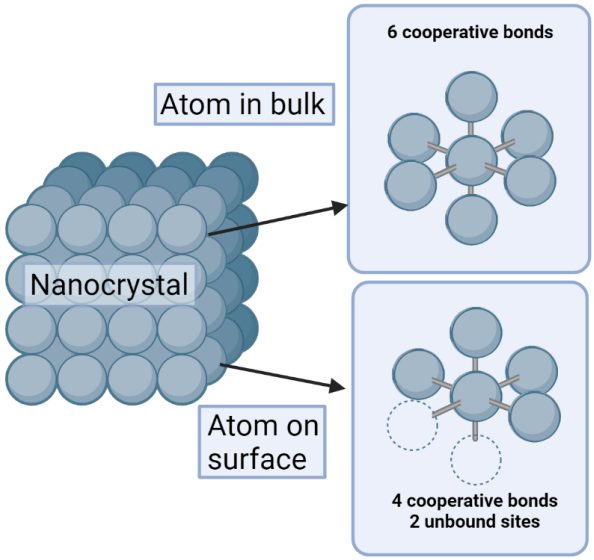

Figure 6. Schematic showing the difference in stabilizing interactions between bulk atoms and surface atoms.

This increase in energy at the surface is also correlated with a higher reactivity. Thus, nanoparticles with a higher percentage of atoms at the surface, will in turn be more reactive. This reactivity influences many different interactions including interactions with surfactants, interactions with other nanoparticles (i.e., aggregation), and interactions with biological molecules (e.g., protein binding).

Measuring Nanoparticle Transformations

Extensive investigations have been carried out to explore the development of ENMs; however, there remains a significant gap in adequately quantifying and comprehending the release and ultimate destiny of these materials. Although various techniques have been employed to measure and analyze nanoparticles, the overall understanding in this field is still relatively underdeveloped. Moreover, these techniques often come with a considerable price tag and necessitate extensive sample preparation to derive meaningful and reliable data.

Table 1 summarizes some of the more common techniques discussed in this section and their benefits and limitations in terms of nanoparticle measurement and analysis.

Table 1. Overview of Measurement Techniques for the Quantification of AgNPs

	ICP-MS[4,18]	AAS[19–21]	SEM/TEM[22,23]	Electrochemistry[3,24,25]
Cost	$$$	$$	$$$	$
Sensitivity	High	Mid-High	High	Mid
Sample preparation	Centrifugation	Centrifugation	Fixation/drying	None
Measurement time	< 1 min	~5 min	>> 10 min	~7 min
Can it measure…				
Ag(I) concentration	✔	✔	✘	✔
AgNP concentration	✔	✔	✔	✔
AgNP size	✘	✘	✔	✔

Current Methods for Size and Surface Charge Determination

In understanding the unique transport phenomena of nanomaterials, the morphology of the particles themselves must be analyzed and understood first. Currently, the common methods for analyzing nanoparticle morphology are electron microscopy, atomic force microscopy, and dynamic light scattering.

In electron microscopy and atomic force microscopy, a direct image of the particles themselves is obtained either via a high-energy electron source (electron microscopy) or a delicate surface probe (atomic force microscopy). In both cases, the actual resolution available with modern equipment is very high and yields images of the nanomaterials that give a detailed understanding of the structure and relative concentration of the nanomaterial sample. However, these snapshots require the sample to be "frozen" or fixed via an elaborate series of drying, solvent exchanging, and cooling. This means that the images obtained via these advanced techniques are static and thus have no real merit in understanding the more complex dynamics of the nanomaterial system. Nevertheless, these techniques are useful for broad characterization.

The other technique commonly employed for the broad characterization of nanomaterials is dynamic light scattering (DLS). In DLS, the particle size distribution is analyzed based on the principle of Brownian motion. Following (A) in Figure 7, a laser is directed at a sample of nanoparticles and some of the photons are scattered back at the detector. The scattering pattering detected at the first time point is then stored and used as a reference to analyze how quickly the signal changes over time. As the particles move away from their initial positions due to random Brownian motion, the scattering intensities detected begin to change.

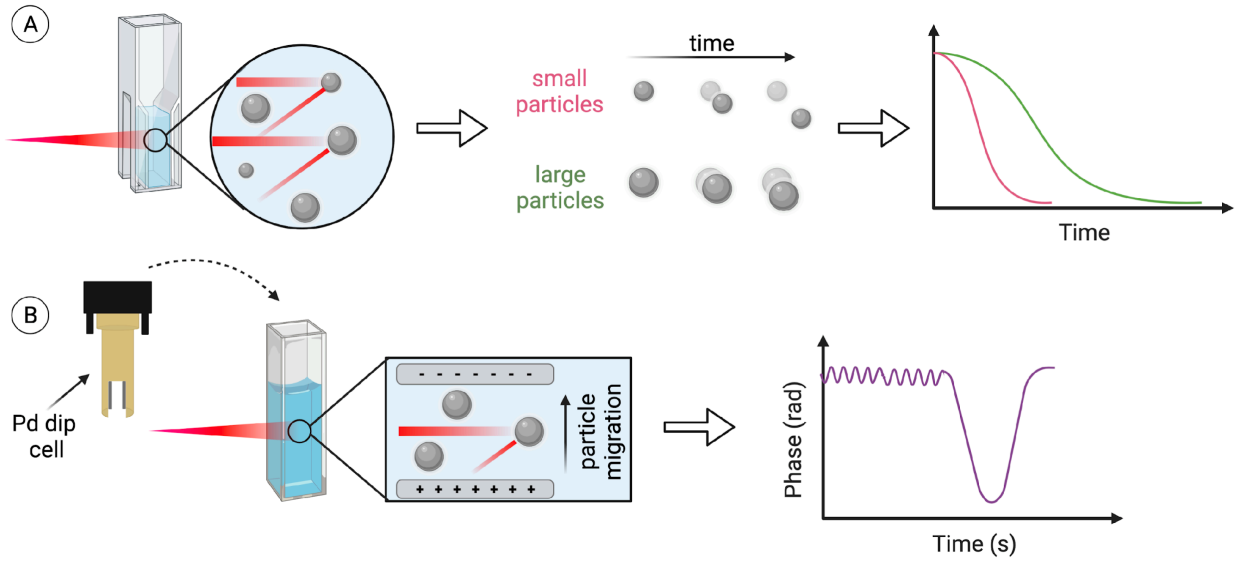

Figure 7: Quantification of nanoparticle size and zeta potential through Dynamic Light Scattering (DLS). (A) Laser light is initially scattered randomly by all particles in solution. As particles diffuse at different rates due to Brownian motion, the scattered signal begins to lose correlation with the initial signal. The rate at which all correlation is lost is proportional to the particle size. (B) Particles are exposed to a known electric potential. The velocity at which a particle diffuses is proportional to its zeta potential.

By performing statistical correlation analyses on the new scattering intensities and the initial scattering intensity, the measured correlation can be plotted over time. The DLS software can then take those correlograms and determine the size of the nanoparticle based on certain preset conditions (e.g., solvent, cuvette type, and temperature). For large particles, which take longer to move from their initial positions, the time it takes for the signal to completely decorrelate is slower than for smaller particles.

Additionally, the DLS-Zeta instrument also allows for the surface charge of the nanoparticles to be analyzed via a palladium dip cell. Following (B) in Figure 7, the dip cell has two oppositely charged electrodes that are submerged into the solution, creating a potential gradient between the two plates. Via electrophoretic flow, charged particles in the solution will be attracted to one side of the electrode pair. Utilizing the same techniques as in DLS, the particle velocities can be calculated. By knowing the electric field strength and

the particle velocity, the Zeta potential (proportional to the surface charge) can be calculated using a series of equations (see Appendix A).

The tandem DLS and Zeta potential measurements are useful tools for determining the size, stability, and aggregation of nanoparticles and have been utilized in determining the binding of biomolecules to the surface of nanoparticles, as well[26]. While the analysis of nanoparticles using DLS is quite effective and measurement times are relatively short, DLS is not able to discriminate between different types of particles. One of the main contributors to this discrepancy is dust particles. For DLS measurements to be well-resolved, the solvent and samples prepared need to be well-filtered. This makes it difficult to use DLS on samples released from embedded materials (i.e., fabric release) or on heavily heterogeneous samples. Additionally, the sensitivity of DLS is not ideal for measuring small changes in size due to surface binding phenomena.

Current Methods for Release/Dissolution Measurement

In addition to the simple characterization of nanomaterials, to fully grasp how nanomaterials evolve and interact with their environment it is necessary to have analytical techniques that offer both high measurement sensitivity and can be repeated rapidly. The current techniques that exist for doing this are either too slow, too destructive, or require the indirect measurement of a certain species.

The most common techniques for doing this analysis are inductively coupled plasma mass spectrometry (ICP-MS)[4,18], flame atomic absorption spectroscopy (FAAS), and graphite furnace atomic absorption spectroscopy (GFAAS)[19–21]. These are all atomic analytical methods, meaning that they are specialized to measure concentrations of specific elements (usually metals) in the sample being analyzed. Due to the one-dimensional nature of these techniques, they cannot be used to directly measure the dissolution/release of nanoparticles.

Instead, they require an additional centrifugation step to separate the in-tact nanoparticles suspended in solution from the dissolved metal ions. Then, once the two species have been separated, the concentration of silver ions in solution can be measured via any of the

aforementioned techniques. Instead of being able to directly analyze the nanoparticle concentration, it is calculated by subtracting the metal ion concentration from the initial concentration of the metal in the sample. This means that all nuanced information about the nanoparticle's size and morphology are not able to be measured.

To truly understand the mechanisms of nanoparticle dissolution and release, a better technique is needed that can accurately measure both the nanoparticles and metal ions directly.

Current Methods for Understanding Nanoparticle-Protein Interactions

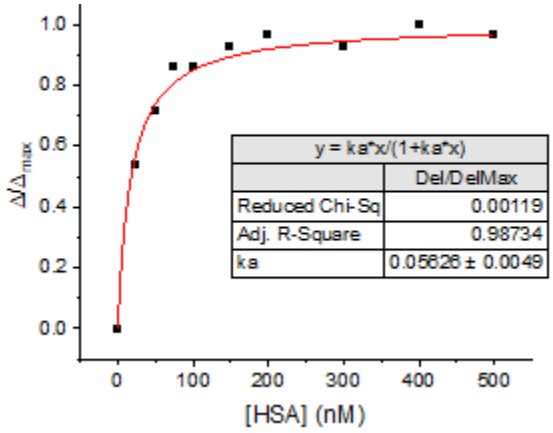

Figure X. Langmuir isotherm of human serum albumin binding to 20 nm silver nanoparticle

The typical way to measure the adsorption of sorbates onto the surface of a nanoparticle is through a Langmuir adsorption isotherm. A Langmuir isotherm utilizes the change in a particular measurement as a function of adsorbate concentration to determine the binding constant of that adsorbate to the surface of a particular material. For measuring the binding of proteins to the surface of a nanoparticle, the change in the LSPR absorbance due to an increase in electron delocalization as a function of protein concentration can be utilized. This change can be observed using a full-width UV-Vis spectrophotometer. A representative isotherm is plotted in Figure 8. Note that the data plotted is fit to the Langmuir isotherm equation given in Equation 3:

$$\frac{\Delta\lambda}{\Delta\lambda_{max}} = \frac{K^*[Protein]}{1+K^*[Protein]} \quad (3)$$

where K is the adsorption constant, $\Delta\lambda$ is the LSPR peak shift, and $\Delta\lambda_{max}$ is the maximum LSPR peak shift. The value for the adsorption of human serum albumin (HSA) to 20 nm AgNPs reported in Figure 8 (5.6×10^7 M^{-1}) is consistent with other findings in my lab as well as in other papers.

Methods

Spectroscopic Techniques

UV-Visible Spectroscopy (UV-Vis)

UV-Visible Spectroscopy (UV-Vis) is a common chemistry technique used for the analysis of molecules (or in this case nanoparticles) and follows the basic principles of photonic absorption. Essentially, molecules and other superstructures absorb energy from photons via the excitation of electrons from a ground singlet state, S_0 (paired electrons have different spins) to an excited singlet state, S_1. This is shown in Figure 9 with a simple Jablonski diagram.

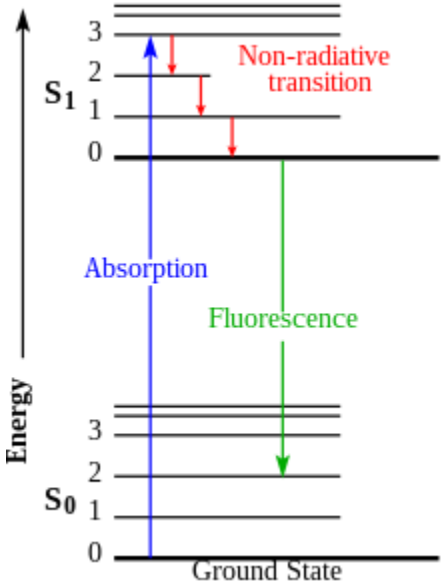

Figure 9. Simple Jablonski diagram showing the excitation (absorption) and relaxation (non-radiative and fluorescence) transitions between two singlet states

The wavelength of light absorbed by this excitation is dependent on a large variety of factors. For nanoparticles, the absorbance of light is due to the LSPR effect discussed above. The larger the nanoparticle, the larger the wavelength of light absorbed. This shift from shorter to longer wavelengths is known as a bathochromic (red) shift. The opposite is called a hypsochromic (blue) shift.

Flame atomic absorption spectroscopy (FAAS)

As described above, flame atomic absorption spectroscopy (FAAS) is a common technique for measuring the concentration of metallic species in samples. It operates similarly to UV-Vis spectroscopy, however, instead of probing molecular absorption, which is often broad and non-specific, the light source probes atomic absorption.

Atomic absorption represents the excitation of an electron from a ground singlet state to an excited singlet state, just like molecular absorption. However, since there are no other ways for the atom to absorb energy (e.g., vibrations, rotations, bending), the wavelength of light at which the atom can absorb is much more narrow. Thus, atomic spectroscopy can be used to analyze multiple different atoms in the same sample.

Even though metal atoms have unique absorption wavelengths, the solvents that they are dissolved in are molecular and thus absorb some of the light when excited by the atomic absorption source. Therefore, for the atomic absorption to be analyzed, the solvent has to be removed. In FAAS, the sample is atomized into a fine mist and passed through a flame where the metal ions are reduced to their atomic form. Then, they pass through the excitation source, and absorption is measured. The concentration is then calculated using an external calibration curve.

Electrochemistry

Electrochemistry takes advantage of a fundamental chemistry principle known as electron transfer. In a system in which electron transfer is enabled, electrons are free to flow to and from certain species, depending on their current states. Electron transfer processes are governed via a type of chemical reaction called a reduction/oxidation reaction (or redox for

short). In a redox reaction, the starting materials react in such a way that there is a transfer of electrons between the substrates to form the products. An example of a redox reaction for a metal M is given in Equation 4.

$$M^{+} + e^{-} = M^{0} \tag{4}$$

Since there is a free electron in this reaction, it is referred to as a half-reaction. In reality, a redox reaction is the combination of two half-reactions where one demonstrates a reductive process (gain of electrons) and the other demonstrates an oxidative process (loss of electrons). The reaction in Equation 4 represents the reduction of metal M.

In electrochemistry, this transfer of electrons can be understood via a principle called the reduction potential (E^{o}). The reduction potential is a characteristic potential (or voltage) for a given electrochemical half-reaction at which equilibrium is reached (i.e., the forward and reverse reactions happen at the same rate). An example redox equilibrium is given in Equation 5a with the corresponding reaction quotient Q described in Equation 5b.

$$Ox + e^{-} \rightleftharpoons Red \tag{5a}$$

$$Q = \frac{[Red]}{[Ox]} \tag{5b}$$

At a cell potential equivalent to the reduction potential, the concentration of reduced and oxidized species is equivalent. This is described mathematically through Equation 5c, also known as the Nernst equation.

$$E = E^{0} + \frac{RT}{zF}\ln(Q) \tag{5c}$$

Where E is the potential of the cell, E^{o}_{cell} is the reduction potential (for the reaction in Equation 5a), Q is the reaction quotient, T is the cell temperature, z is the number of electrons transferred, and R and F are the molar gas constant and Faraday's constant, respectively.

Upon further analysis of the Nernst Equation, at potentials below the reduction potential, the reductive products are favored, and at potentials above the reduction potential, the oxidative products are favored. The relationship between the reaction quotient and cell potential is displayed in Figure 10. Importantly when E is above E^o, Q is greater than one and when E is below E^o, Q is less than one.

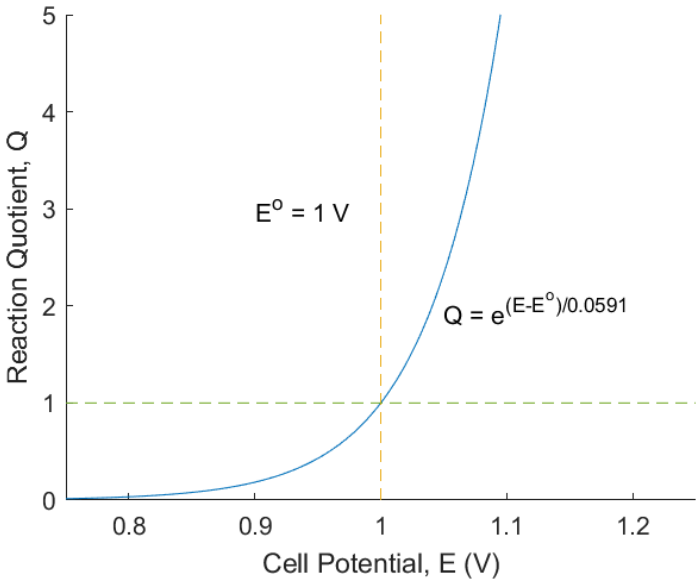

Figure 10. Plot of an example cell reaction quotient, Q, as a function of the applied cell voltage, E. Here, the reduction potential of the system is 1 V, assuming a temperature of 298 K and one electron transferred.

In electrochemical methods, the relationship between cell potential and the ratio of oxidized and reduced products (Q) allows for a wide range of applications based on the species being measured and the methods utilized. Herein, the use of two different electrochemical methods will be discussed: linear sweep stripping voltammetry and particle impact voltammetry.

Linear Sweep Stripping Voltammetry (LSSV)

Linear sweep stripping voltammetry (LSSV) is an electrochemical technique that allows for the measurement of ionic concentrations of certain metals based on their reduction potential when compared to a reference electrode. A sample is prepared by loading a solution into an electrochemical cell and adding a working electrode, reference electrode, and counter electrode all connected to a potentiostat as shown in Figure 11.

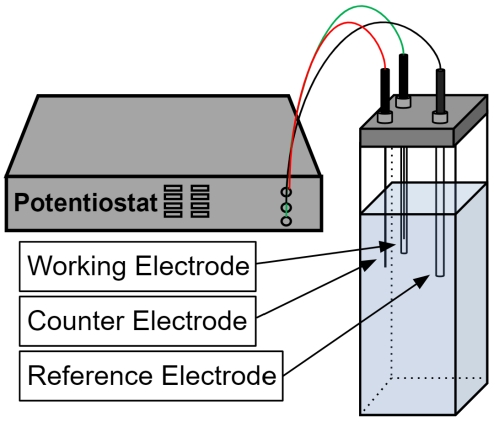

Figure 11. Electrochemical electrode setup for both linear sweep stripping voltammetry and particle impact voltammetry

For extra sensitivity, a picoamp booster can be added between the electrodes and the potentiostat. To start the measurement, the sample is held at a reducing (deposition) potential well below the actual known reduction potential for 60 seconds. After the deposition period, the potential on the sample is swept from the high reducing potential through the reduction potential and slightly past, to ensure complete oxidation of the previously reduced substrate back to the oxidized form. This oxidation is observed as a peak in the current vs potential (i-V) plot (Figure 12). By integrating this peak and comparing it to a standard calibration curve, the concentration of the metal ion in the solution can be determined.

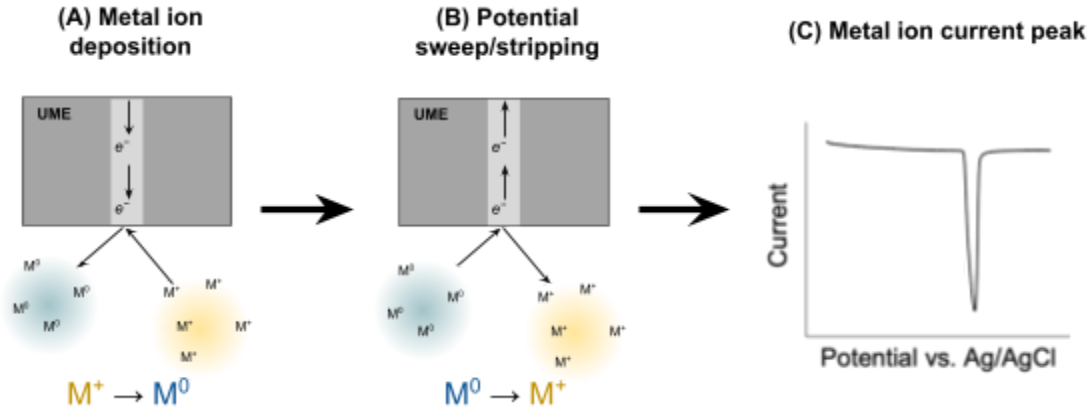

Figure 12. Linear sweep stripping voltammetry schematic showing interaction between metal ions and the UME surface during (A) deposition and (B) the potential sweep. (C) Metal ion peak in the i-V plot.

LSSV has been used as a reliable way to measure both singular and multiple metallic ions in relatively clean solutions for decades.[27] It is specifically designed for this type of analytical application due to the enhanced sensitivity garnered from the deposition step. Instead of relying on the slow time-limited diffusion of ions to the electrode's surface, using a deposition period allows for the system to be charged up over time, thus yielding a much larger signal when the system is reverted to equilibrium (after the potential sweep). Additionally, the unique reduction potentials of most metals can allow for the analysis of multiple metallic ions at the same time. This is shown in work done by T. M. Florence where he demonstrated the separation of four different metallic ions in a potassium nitrate solution (Figure 13).[28]

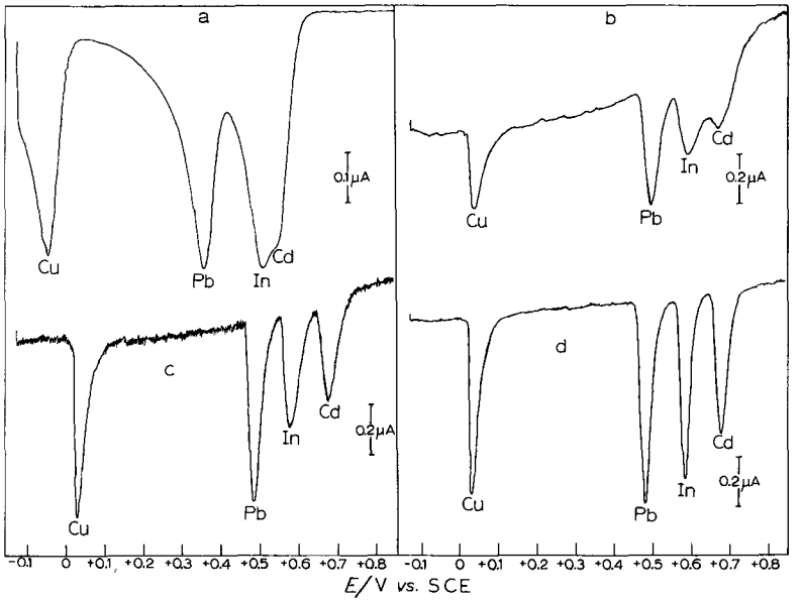

Figure 13. Stripping curves showing the distinct separation of four metallic ion signals: Cu^{2+}, Pb^{2+}, In^{3+}, and Cd^{2+}. [From T. M. Florence, *J. Electroanal. Chem*, **27**, 273 (1970), with permission]

Particle Impact Voltammetry (PIV)

Particle impact voltammetry (PIV) works opposite to LSSV, where the species of interest is now a non-ionized metallic atom. This means that instead of having to reduce the substrate

to measure the electron transfer, the nanoparticle needs to be oxidized. For an oxidative process to occur, the cell potential must be greater than the reduction potential. The magnitude above the reduction potential will determine the kinetics of this process. In PIV, a large oxidizing potential is used to selectively oxidize single nanoparticles through the oxidation half-reaction shown in Equation 6.

$$M^0 \rightleftharpoons M^+ + e^- \quad (6)$$

However, instead of measuring the oxidation of a single atom, the entire nanoparticle will be oxidized to M^+. This process is achieved through a working ultramicroelectrode held at a high oxidizing potential. Since this potential is much larger than the reduction potential of the metal, we expect any nanoparticles that come into contact with the electrode to be fully oxidized. This schematic is shown in Figure 14a.

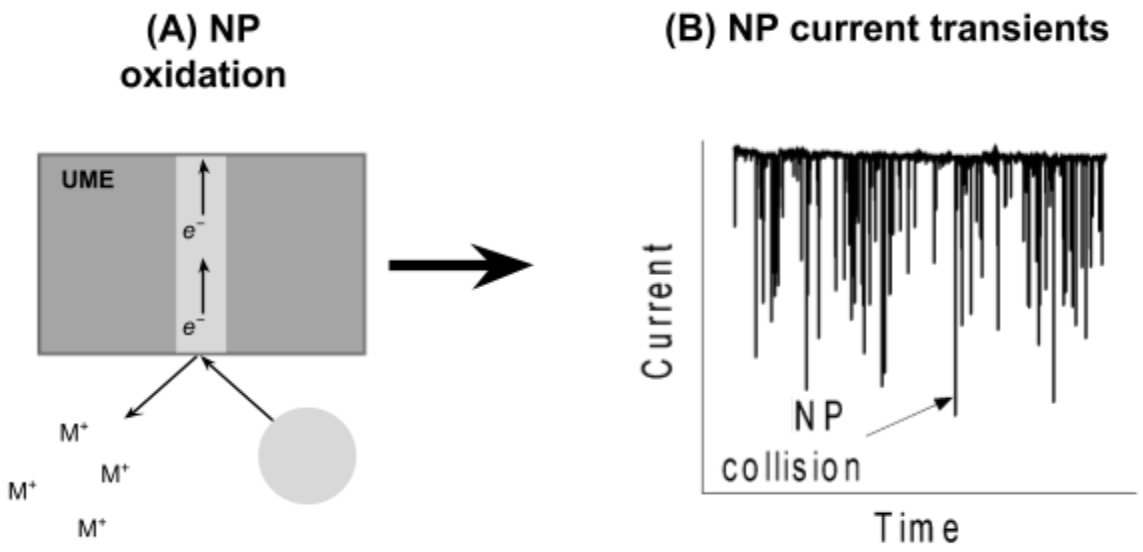

Figure 14. (A) Particle impact voltammetry schematic showing interaction between a nanoparticle and the UME surface and (B) the corresponding nanoparticle impact current transients over time.

Over the measurement period, any nanoparticles that impact the working electrode are detected as a current transient in the current vs time (i-t) plot (Figure 14b). This is due to the idea of complete nanoparticle oxidation. As a metal nanoparticle impacts the electrode surface, the metal atoms immediately in contact with the electrode are oxidized (i.e., lose an electron) to M^+. At this point, the electromotive force of the large potential difference causes

a chain reactive flow of electrons from farther out metal atoms in the nanoparticle. This causes a time-stamped spike in current in the i-t curve associated with the complete oxidation of that single metal nanoparticle. By integrating that transient, total charge, Q, transferred can be measured,

$$Q = \int i dt \tag{7a}$$

That can then be related to the number of metal atoms, N, in the nanoparticle.

$$N = \frac{Q}{e} \tag{7b}$$

Where e is the charge of an electron (1.602×10^{-19} C). Using this data, the diameter of the nanoparticle, D_{np}, can be determined using the following equation (proved in Appendix B):

$$D_{np} = 2 \cdot \sqrt[3]{\frac{3A_r N}{4\pi N_A \rho}} \tag{7c}$$

where A_r is the relative mass of the metal, N_A is Avogadro's number, and ρ is the density of the metal[29]. The concentration of nanoparticles is also able to be measured by analyzing the frequency of transients (i.e., how many nanoparticle peaks are observed over the measurement duration). This is then compared to a calibration curve to determine the concentration of nanoparticles in the solution.

PIV is less of a commonplace technique than LSSV. The use of nanoparticles in electrochemical systems is also a relatively new idea, sparking interest after a paper published in 1995 titled *Polarography and Voltammetry of Ultrasmall Colloids: Introduction to a New Field*.[30] However, most of the work done using nanomaterials and colloids focuses on the bulk sample, rather than the individual particles. This is mainly due to the lack of equipment sensitive enough to measure individual nanoparticles. Moving forward about ten years later, Bard et. al. published the first observations of an interaction between the working electrode and single nanoparticles.[31] In this publication, Bard reports the observation of platinum nanoparticle impacts with an ultramicroelectrode. Now, the technique is finally being utilized for more complex nanomaterial characterizations.

Herein, PIV will be utilized in manners not shown throughout the literature. Due to the nature of these new, sensitive methods, the design and method optimization reported will show significant progress in the field of nanoparticle electrochemistry. This also means that a lot of the optimization aspects have not been fully flushed out and thus would require further work to complete in their entirety.

Results and Discussion

Project 1: Release Dynamics of AgNPs and Ag(I) from Embedded Textiles

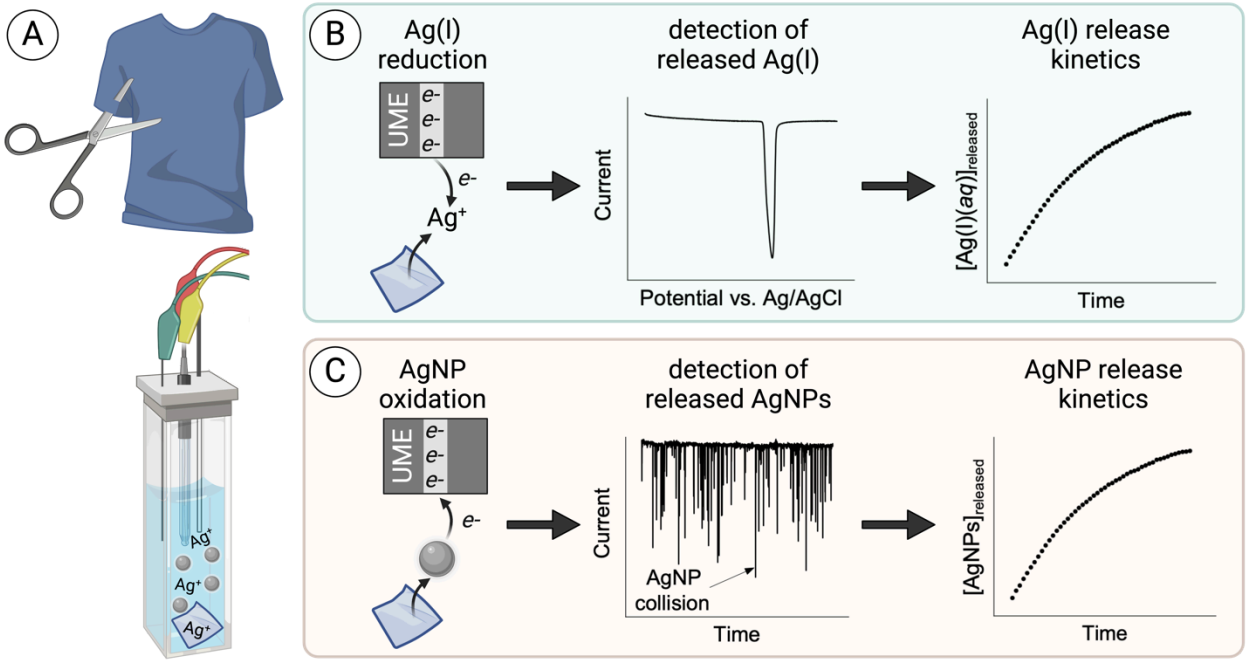

Figure 15. Real-time quantification of the release of AgNPs and Ag(I) from AgNP-embedded textiles using LSSV-PIV. (A) An AgNP-embedded textile is placed into a glass cuvette. (B) The concentration of Ag(I) is determined through LSSV. (C) Immediately following LSSV, PIV is used to determine the concentration and size of AgNPs released from the textile. This is repeated 36 times over four hours.

Preliminary Idea

After discovering techniques for measuring both metal ion concentration (LSSV) and metal nanoparticle concentration (PIV) using the same instrument, the most logical next step is to see if these two techniques could be coupled together. This preliminary idea would allow for a simple, inexpensive technique that could analyze the kinetics of nanoparticle release,

diffusion, and aggregation completely *in-situ* of a nanoparticle-containing fabric. This is a result that nobody has been able to achieve so far in the literature.

To do this, a new methodology needed to be developed to both allow for the techniques to be run sequentially and for the coupled techniques to be repeated over the course of multiple hours. A schematic representation of this methodology is given in Figure 15 and the nuanced technical parameters and experimental set-up will be discussed in the following sections.

Constraints and Requirements

For this project, the constraints were as follows. The sensitivity of the instrument needed to be high enough to detect both the transients of the nanoparticles measured as well as the current peaks of the silver ions measured. Additionally, the instrument needs to maintain this sensitivity over a four-hour measurement period. Also, the fabric utilized can not interfere with the measurement or else the data obtained would not be reliable or reproducible. Finally, the cost is a large constraint here. Without the resources that are already in the lab, the project would cost approximately $10,000 starting from the ground up.

Now, to assess the method designed herein, there were three main requirements that needed to be met. They are as follows:

1) The method needs to allow for the measurement of both AgNPs and Ag(I) concentrations released from AgNP-enabled textiles. The measured concentrations must also be within the limit of detection (LOD) of the calibration method utilized.
2) The method needed to allow for the construction of time-dependent concentration plots to understand the release kinetics of both AgNPs and Ag(I) over time as well as the correlation between the release of the two species.
3) The method must be reproducible across different sweat conditions, different fabrics, and over different days.

Design and Optimization

To start, the instrumental set-up needed to be optimized to allow for access to external heating and to modify the electrochemical cell stand to include a picoamp booster to increase the instrumental sensitivity. This set-up was in place before this project was started and an image of the final set up is provided in Figure 16.

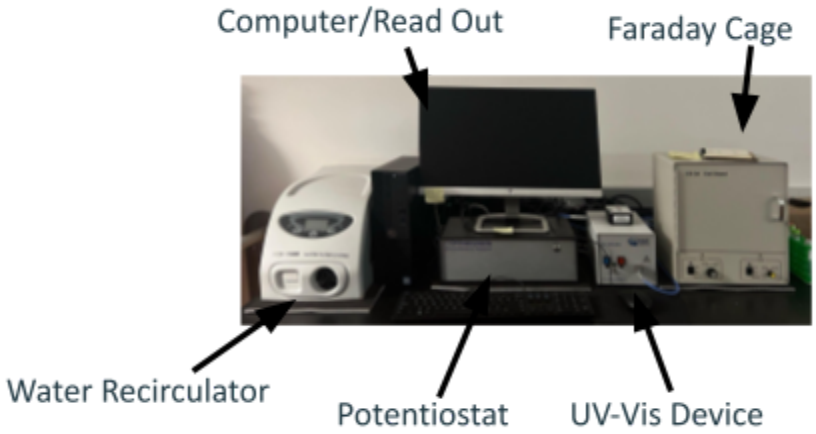

Figure 16. Layout of electrochemical analyzer with optional UV-Vis spectrometer and temperature controller

The electrochemical instrument includes a Faraday cage the houses the electrochemical cell holder, a potentiostat that connects to the cell through a picoamp booster at the back of the faraday cage, a water recirculator that cycles water at a certain temperature through the cell stand to control the cell temperature, and a desktop that displays the data relayed through the potentiostat. Additionally, a micro UV-Vis device was added and allows for the direct analysis of the sample in the electrochemical cell via UV-Vis spectroscopy. This was not utilized in the fabric measurement design, but will become important in the design of the protein binding assay.

In addition to the instrumentation, the working electrode (11 um carbon fiber electrode) needs to be maintained via daily polishing. To be more consistent with day-to-day polishing, a machine polishing set-up was designed with a speed-controlled rotating disk polisher and a digital microscope purchased off of Amazon. This design is pictured in Figure 17a. The magnification of the microscope was adjusted to keep both the tip of the electrode and the polishing pad in focus (Figure 17b).

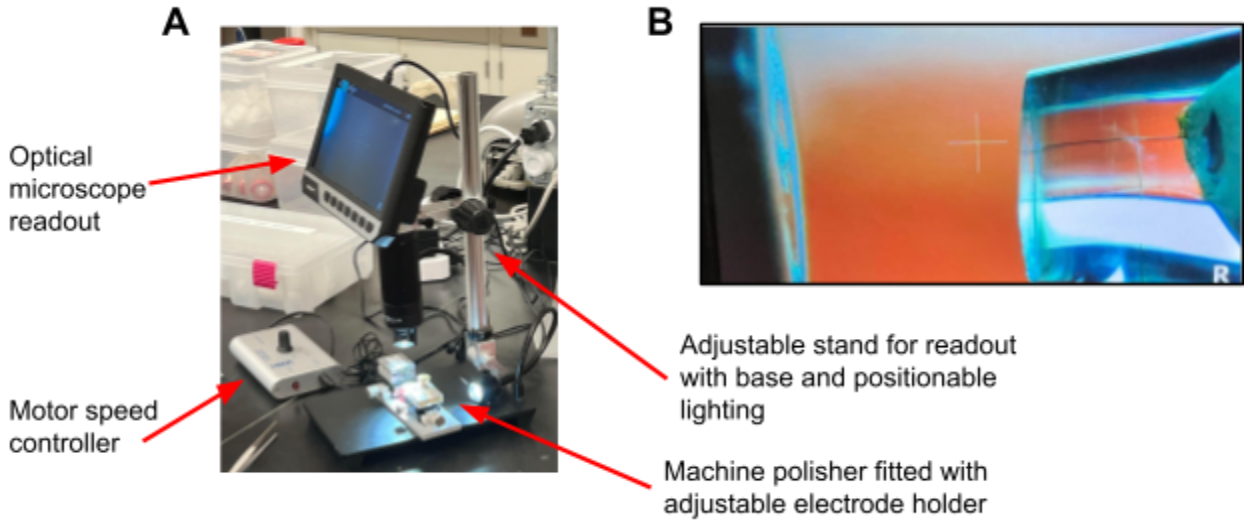

Figure 17. (A) Layout of machine polishing setup and (B) an example image of a carbon fiber ultramicroelectrode nearing the polishing surface.

In this set-up, the electrode's surface can be polished controllably and yield more consistent electrochemical results.

Table 2. LSSV parameters for Ag(I) concentration determination

Initial Potential	-0.5 V
Final Potential	0.5 V
Scan Rate	0.05 V/s
Sample Interval	0.005 V
Sensitivity	1.e-009 A/V
Stripping Mode	Enabled
Deposition Potential	-0.5 V
Deposition Time	60 s

With the instrument and equipment set up, the next step was to optimize the experimental conditions. This includes both the instrumental parameters as well as the solution and sample conditions. Starting with the instrumental parameters, there are a lot of possible variables that can be adjusted. Since LSSV was already a well established technique in the

lab, the instrumental parameters utilized were already well optimized. These parameters are included in Table 2.

Using these parameters the cell will undergo a 60-second deposition at -0.5 V (below the reduction potential of silver), then the current will be swept from -0.5 V to 0.5 V at 0.5 V/s. The final voltage of 0.5 V was chosen as it is sufficiently higher than the reduction potential of silver (~0.15 V when compared to a Ag/AgCl reference electrode) and because it matched the PIV voltage, as described below.

However, the parameters for the analysis of AgNPs using PIV still needed to be optimized. Although there are only three instrumental parameters that can be varied (potential, measurement duration, and measurement rate), there are additionally more experimental choices that allow for the quality of the PIV signal to be optimized.

The oxidation potential was optimized first. The potential was varied to gain an understanding of how the nanoparticles reacted to different voltages. The idea was to analyze how far away the potential needed to be from the reduction potential to still yield enough PIV signal. A representative depiction of this analysis is given in Figure 18.

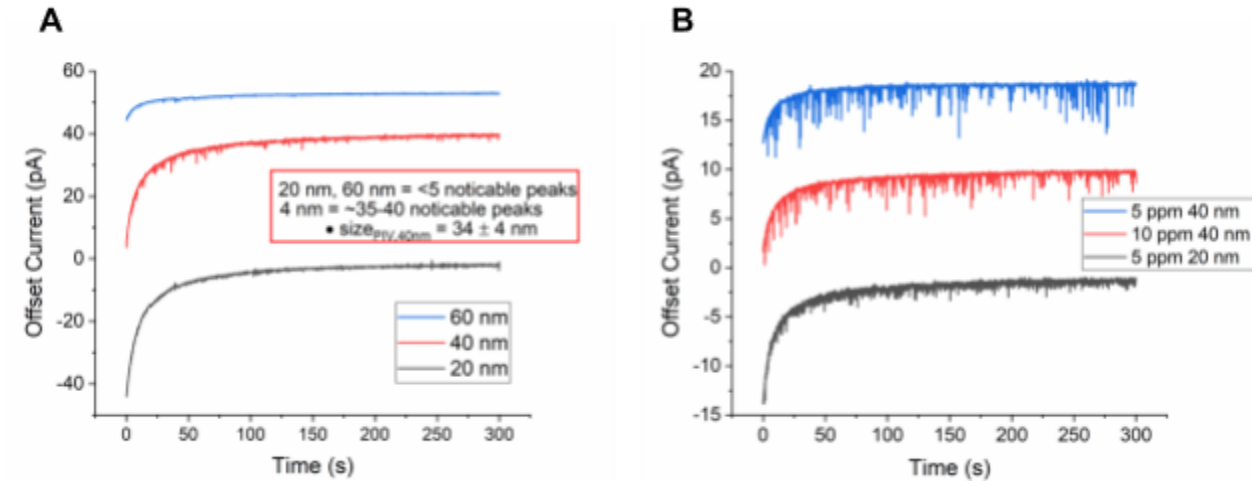

Figure 18. Effect of different oxidizing potentials on the PIV measurement. AgNP samples of different sizes were analyzed with an oxidizing potential of either (A) 0.8 V or (B) 0.5 V. Analysis was performed in a 10 mM NaCl, 10 mM sodium citrate buffer at pH 5.

In Figure 18, the oxidizing potential was kept at either (B) 0.5 V, which is somewhat above the reduction potential, or (A) 0.8 V, which is substantially higher than the reduction potential. If the oxidation of the particles truly scaled proportionally with an increase of the oxidation potential (as is theorized), then more signal would be expected with a 0.8 V potential. However, this is the opposite of what truly happened. At 0.8 V the nanoparticle signal was significantly quenched when compared to the results at 0.5 V.

This result is mainly due to the fact that, at a large overpotential (0.8 V), the electrode becomes too reactive that it both loses the oxidative selectivity that allows for the complete oxidation of the particles and starts to degrade much quicker. This means that the surface of the electrode becomes covered with oxidized silver and other species and can no longer be used for PIV without being re-polished. A good analogy for this would be a circuit box rated for a certain amount of current flow. If the current flowing greatly exceeded the maximum allowable by the fuse box, then the circuit would short and the fuse would need to be replaced. So, from this analysis, the oxidation potential was set to 0.5 V for all of the fabric-release PIV analyses.

Now, after the oxidation potential was chosen, the consistency between different runs was not fully reproducible. There were a few factors that could have been impacting this. The first that stood out was whether or not the solution was being stirred. A paper was published in 2016 that reported an interesting finding about the importance of stirring when running PIV. As is shown in Figure 19, the transient frequency is greatly increased when stirring was enabled (down arrows)[32]. The effect of stirring was performed on the system being used in this report and it seemed to not have a significant effect, however.

Additionally, due to the small cell that's being used, the stirring actually had the adverse effect of increasing the amount of noise in the system. With this, as well as the fact that the system would be much more difficult to understand with both a stir bar and a fabric sample at the bottom of the cuvette, it was decided not to stir the sample during the release experiments.

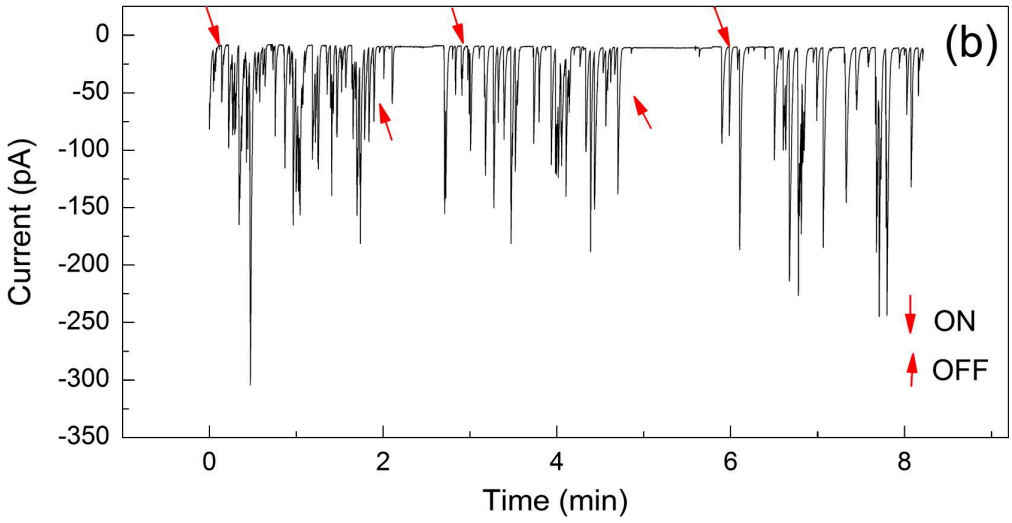

Figure 19. Current-time plots showing the impact of stirring on the PIV signal of 25 nm PtNPs. The arrow direction indicates when stirring was turned on and off. [J. Jiang et al. / Journal of Colloid and Interface Science 467 (2016) 158–164, with permission]

Moving on to the full release experiment, there were two methods that needed to be developed: the release experiment itself and the in-between run cleaning. Starting with the release experiment, the simplistic representation is as follows. The Ag(I) concentration is first measured via LSSV (~1 min 15 sec), then the AgNP concentration is measured via PIV (~5 minutes), and finally, the voltage is swept back to the starting LSSV deposition potential to reset the system. The change in voltage over time for a single release measurement is given in Figure 20. This process takes approximately seven minutes and thus can be cycled 36 times through the course of a 4-hour release period. The full annotated macro command for this process is in Appendix C.

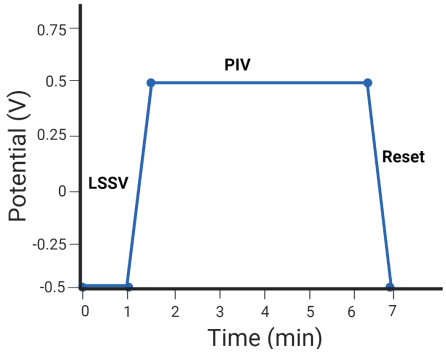

Figure X. Change in voltage over time for a single fabric release measurement.

After the full-length experiment was designed, there were still issues with the consistency between successive experiments. This can be attributed to the degradation of the electrode surface over time. Even at an oxidizing potential that should not damage the electrode (0.5 V), oxidized silver can build up on the electrode's surface over the measurement period. Because of this, an in-between measurement cleaning procedure needed to be designed. This procedure is outlined in Figure 21.

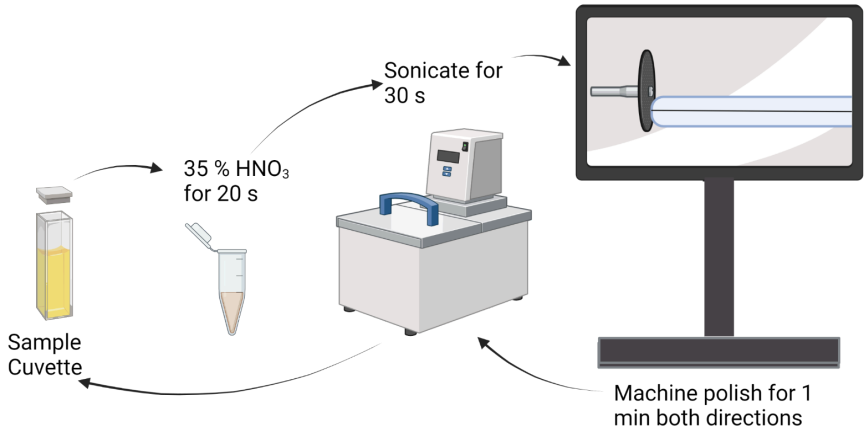

Figure 21. Schematic representation of the cleaning performed in between each four-hour fabric release experiment

After the sample is finished running, the working electrode is taken out of the sample cuvette and placed in a solution of 35% nitric acid for 20-30 seconds. This step effectively redissolves any silver stuck to the electrode surface, turning it into silver nitrate. Then, the electrode is sonicated for 30 seconds to dislodge any further stuck-on oxidized contaminants and machine polished for a minute in each direction to 'reset' the electrode for the next measurement. Additionally, while the working electrode is being cleaned, the reference electrode, counter electrode, and sparge tube are all rinsed with Millipore water to ensure no silver species transfer into the next cell.

Table 3. Composition of simulated sweat (SSW) solutions

	[NaCl] (%w/v)	[lactic acid] (%v/v)	[urea] (%w/v)	pH
SSW1	0.05	0.1	0.1	4.5
SSW2	0.05	0.1	0.1	6.5
SSW3	0.50	0.1	0.1	4.5

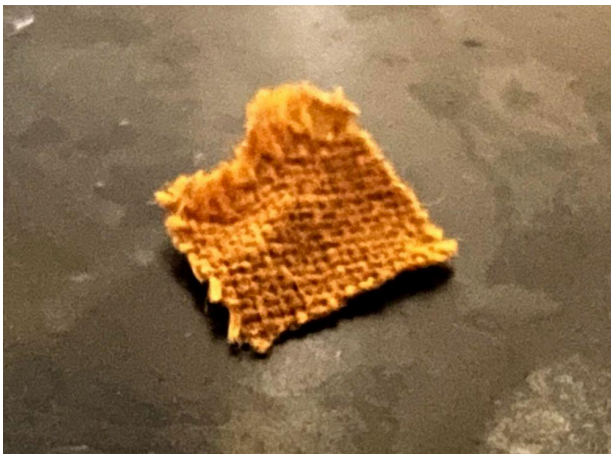

Figure 22. 0.5 cm x 0.5 cm swatch of silver-enable fabric used for the release study

At this point, the experimental method was completely optimized and ready for actual analysis. For ease of experimental design, the variables chosen to analyze this method were the solvent, pH, and NaCl concentration. The three different simulated sweat solutions tested are outlined in Table 3. Additionally, to ensure that the results were consistent for each measurement, the fabric samples (pictured in Figure 22), were always cut to the same dimensions (0.5 cm x 0.5 cm).

Results and Discussion

Once the entire method was optimized and fully designed, testing could begin to validate the technique and ensure that the measurements collected met the requirements set at the beginning of the project. Figure 23 shows the results from three different fabric release measurements in different sweat conditions at body temperature (37 C). From the plots in Figure 23a, it is clear that both the AgNPs and Ag(I) concentrations were able to be measured over time[1]. This is further corroborated in Figure 24 as the final concentrations of AgNPs and Ag(I) were also determined.

[1] As a note, all concentrations are reported as a percent of the total loaded Ag as determined using FAAS

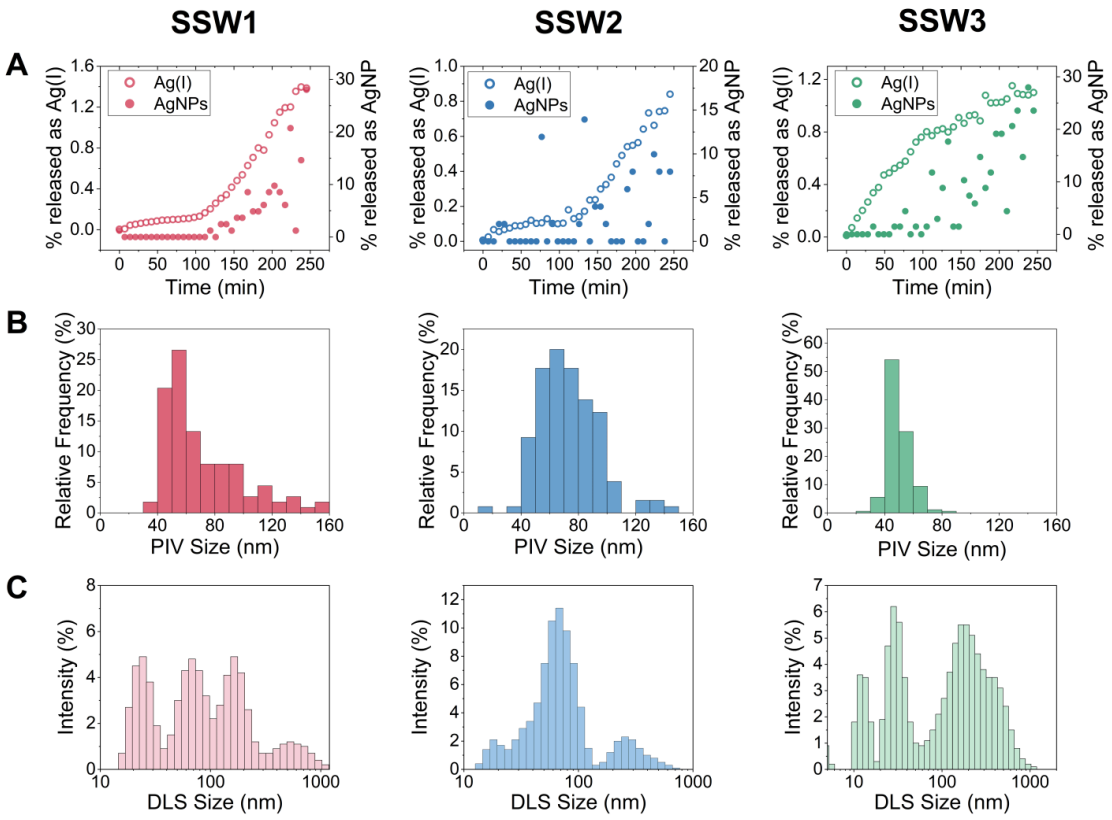

Figure 23. (A) Ag(I) and AgNP release curves measured using LSSV and PIV, respectively, over 4h. Size distributions of released AgNPs were measured using (B) PIV and (C) DLS at t = 4h. Data was collected at 37 C in either SSW1, SSW2, or SSW3.

Additionally, each plot shows a correlation between the start of the nanoparticle release and an increase in the rate of Ag(I) released. This trend is most visually obvious for SSW1. In plot SSW1A, the percentage released of total silver as Ag(I) starts relatively slow (from 0 to 100 minutes). Then, as the release of AgNPs begins to be detected (around 100 minutes), the release of Ag(I) increases drastically. This is expected as the released AgNPs yield an increase in the surface contact between the AgNPs and the solvent when compared to AgNPs stuck in the fabric matrix of the textile. This increase in surface contact leads to a higher relative activity of the ions surrounding the nanoparticles and thus, they will begin to dissolve faster. This trend is also seen in the other two sweat conditions.

Using PIV, the average size of the nanoparticles was also obtained. From the histograms of average PIV size in row B, it can be seen that the average size of the particles was

approximately 60 nm, as expected. However, when compared to other size data taken of the samples after the measurement period (row C), there seems to be a level of detail missing from the PIV data. This is due to the nature of PIV as a diffusion-limited technique. Essentially, when the AgNPs begin to aggregate over time in solution, their sizes increase and they become slower to diffuse. This means that the effective concentration of these aggregated species is low using PIV when compared to the calibration curves using 60 nm particles. However, since these aggregated species do not make up a substantial amount of the AgNP makeup, they are not as relevant for the release studies, directly.

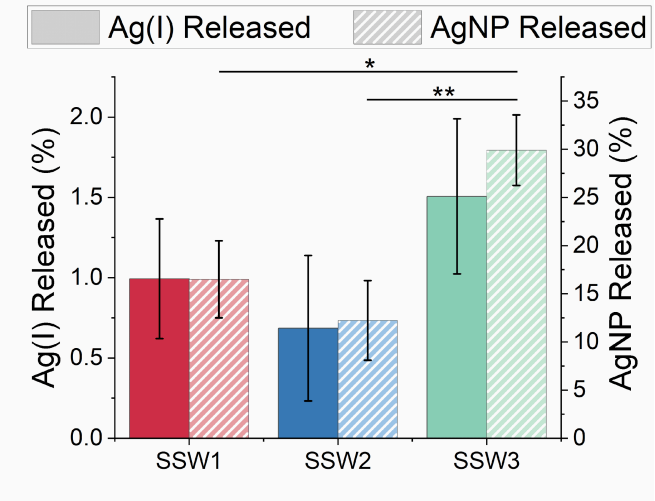

Figure 24. Percentages of Ag(I) and AgNPs released from a 0.5 x 0.5 cm swatch of an AgNP-embedded textile into various SSW solutions. Experiments were performed at 37 °C and percentages represent the total amount of Ag(I) and AgNPs released after 4 h relative to the total amount of Ag initially in the textile. Statistical significance was determined using a two-tailed t-test evaluated at the 95%(*) or 99%(**) confidence level.

On top of the individual measurements for each of the sweat conditions shown in Figure 23, Figure 24 also demonstrates that this technique is reproducible across each salt condition. From the error on each bar, the data remained about as consistent as expected due to the natural error between each fabric sample (i.e., fabric fraying, surface area, and loading inconsistencies). This is furthered by the release data in SSW3 having an overall higher release than the other two SSW conditions. This makes sense as SSW3 has the highest salt concentration and thus the largest ionic strength and activity, leading to more dissolution and charge mobility.

From all of these results, it can be concluded that this technique was sufficiently able to meet each of the three requirements set for the measurement capabilities. Thus this design offers a successful way to analyze materials embedded with AgNPs at a fraction of the cost of other, narrow-ranging techniques.

Project 2: Understanding Protein Interactions with AgNP

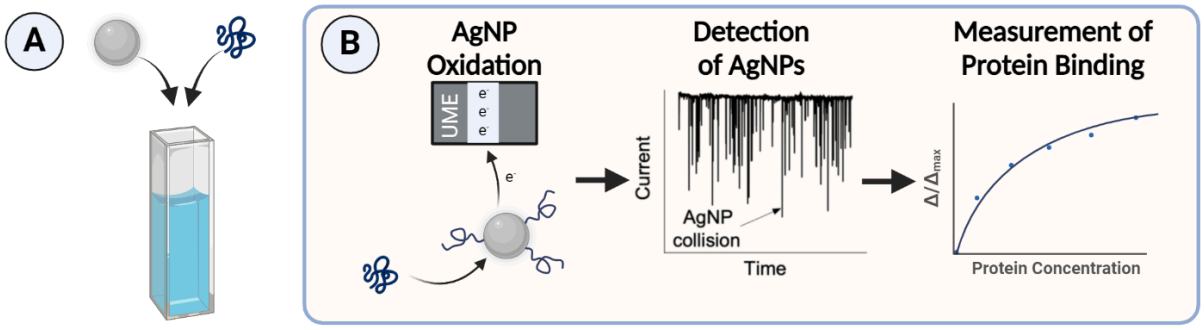

Figure 25. Langmuir protein adsorption schematic using PIV. In (A), the protein and nanoparticle are introduced, interact, and then (B) the PIV signal is measured as a function of the protein concentration added and a Langmuir isotherm is derived.

Preliminary Idea

With the successful analysis of nanoparticle-enable fabrics via LSSV and PIV, the next reasonable direction was to analyze what happens to a nanoparticle after it is released into the environment. This open-ended prompt can be simplified into the following question:

How can we measure the interaction between nanoparticles and biological molecules using electrochemistry?

As discussed previously, there are established methods for analyzing nanoparticle adsorption using Langmuir isotherms and UV-Vis spectroscopy. However, these Langmuir isotherms are not technique specific. Looking back at Equation 3, the measured quantities used to solve for the binding constant are normalized changes in signal rather than absolute measured values. This means that Langmuir adsorption isotherms can be utilized

for any analytical method where there is a measurable change in signal upon the binding of the biological molecule.

Therefore, if there is an electrochemical method where a change in signal can be measured upon the addition of biological molecules, it can be used to analyze the nanoparticle-biomolecule interaction. The technique chosen to do this was PIV.

In theory, upon the addition of biomolecules onto the nanoparticle surface, the diffusion of the particles should be slowed and the number of transients measured should decrease. The underlying scheme of this method is given in Figure 25 and the optimization of this technique and preliminary results are presented in the following sections.

Constraints and Requirements

For this project, the constraints were as follows. The sensitivity of the instrument needs to be high enough to measure the transients of the nanoparticles measured. Also, the proteins added to the nanoparticles can not interfere with the electrochemical measurement, or else the data obtained would not be reliable. Finally, the cost is a large constraint here. Without the resources that are already in the lab, the project would cost approximately $10,000 starting from the ground up.

Now, to assess the method designed herein, there were three main requirements that needed to be met. They are as follows:

1) The method needs to allow for the detection of protein-nanoparticle interactions via a change in PIV signal.
2) The method needed to allow for the determination of protein-nanoparticle binding constants via a change in PIV signal as a function of protein concentration. This would then be fit using a Langmuir isotherm.
3) The method must yield results similar to other techniques previously utilized within a similar analysis time frame.

Design and Optimization

Moving into this project, the same experimental setup as Project 1 was utilized. The only major differences between the two projects were the sample preparation, PIV optimization, and results analysis performed.

Starting with the sample preparation, this step followed closely to what some other methods utilized in the Riley Lab, but was more geared towards electrochemical analysis. The relevant buffer for this method was a citrate-salt buffer with varying concentrations of both sodium citrate and sodium chloride. This is a common buffer utilized for silver nanoparticle analysis as the colloids are already suspended in a citrate solution and the salt assists in ionic strength and charge mobility (for electrochemistry). As is shown in Figure 26, Langmuir isotherms of human serum albumin (HSA) and 20 nm AgNPS were performed in two different salt concentrations (5 and 20 mM) using both a benchtop UV-Vis and the UV-Vis incorporated into the electrochemical setup. These salt concentrations represented the low and high end of the buffers that would be tested.

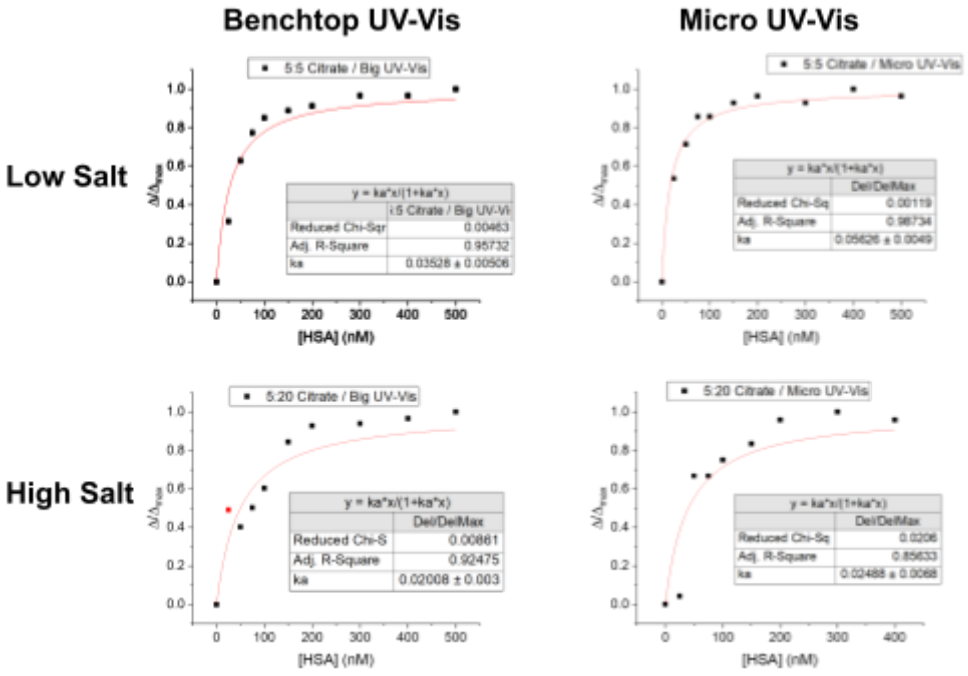

Figure 26. UV-Vis Langmuir adsorption isotherms under two different salt conditions: low (5 nM NaCl) and high (20 nM NaCl) concentrations. Each Langmuir was performed both on the regular benchtop UV-Vis and the Micro UV-Vis designed to work inside the electrochemical analyzer.

To ensure that there was a high enough salt concentration to allow for proper PIV measurements and to properly stabilize the particles in the solution, a final buffer concentration of 10 mM Citrate and 10 mM NaCl was selected for this method design. Additionally, the pH of the buffer solution was adjusted to approximately 4.5 to be consistent within each run (recall from Project 1 that pH did not have a significant effect on the AgNPs).

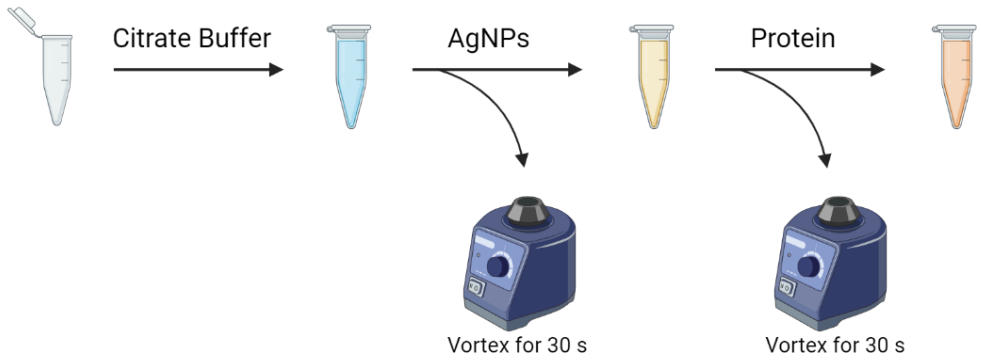

Figure 27. Sample preparation schematic of protein-nanoparticle samples

Once the buffer solution was chosen, a sample preparation had to be designed to properly allow for the incorporation of both AgNPs and proteins into the sample cuvette as well as proper incubation time for binding equilibration. Figure 27 shows the final preparation schematic where the substituents are added in the following order: 1) Buffer, 2) AgNPs, 3) Protein. This order was decided by trial and error and makes intuitive sense. The buffer must be added first or the concentrations of the AgNPs, proteins, or both would be significantly higher than expected. This could lead to aggregation or increased activity than expected. After the buffer has been measured and added, the AgNPs and proteins can be added in either order, but starting with AgNPs mimics them being released into the environment first and then interacting with a protein.

Importantly, after the addition of both AgNPs and the protein, the sample vials need to be vortexed to fully homogenize the sample before moving on. Once the samples were made

they were left to sit at ambient temperature for at least 30 minutes to allow the complete AgNP-protein equilibrium to be established.

The volume of each substituent used was also calculated and measured for each differing concentration of AgNP and protein. Herein, the concentration of 20 nm AgNPs utilized was kept constant at 5 ppm and the HSA/BSA concentration was varied from 0 to 500 nm (0, 25, 50, 75, 100, 250, 500 nM). These concentrations were chosen as they were shown to yield successful Langmuir isotherms when utilizing UV-Vis (see Figure 26).

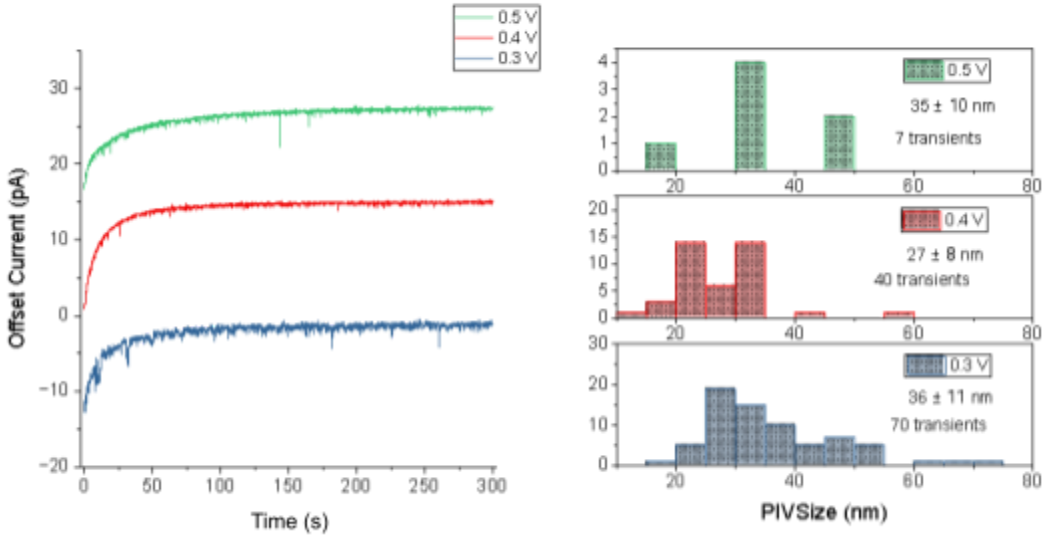

Figure 28. Oxidation voltage optimization using 20 nm particles. (Left) The representative PIV i-t curves for 0.3, 0.4, and 0.5 V are given as well as (right) the size distributions for each voltage.

After the sample preparation was completely designed, the only experimental parameter left was the PIV optimization. Remembering back to Project 1, the only instrumental knobs to turn for PIV are the oxidizing voltage and the measurement interval. Similarly to project 1, the measurement interval was kept constant at 0.1 s to minimize the instrumental noise. However, since this project revolved around 20 nm particles, the optimal oxidizing voltage was different. As is shown in Figure 28, it turned out that the most consistent voltage to use was 0.4 V. This allowed for enough signal to be measured without leading to too much noise (0.3 V tended to be noisier for some reason).

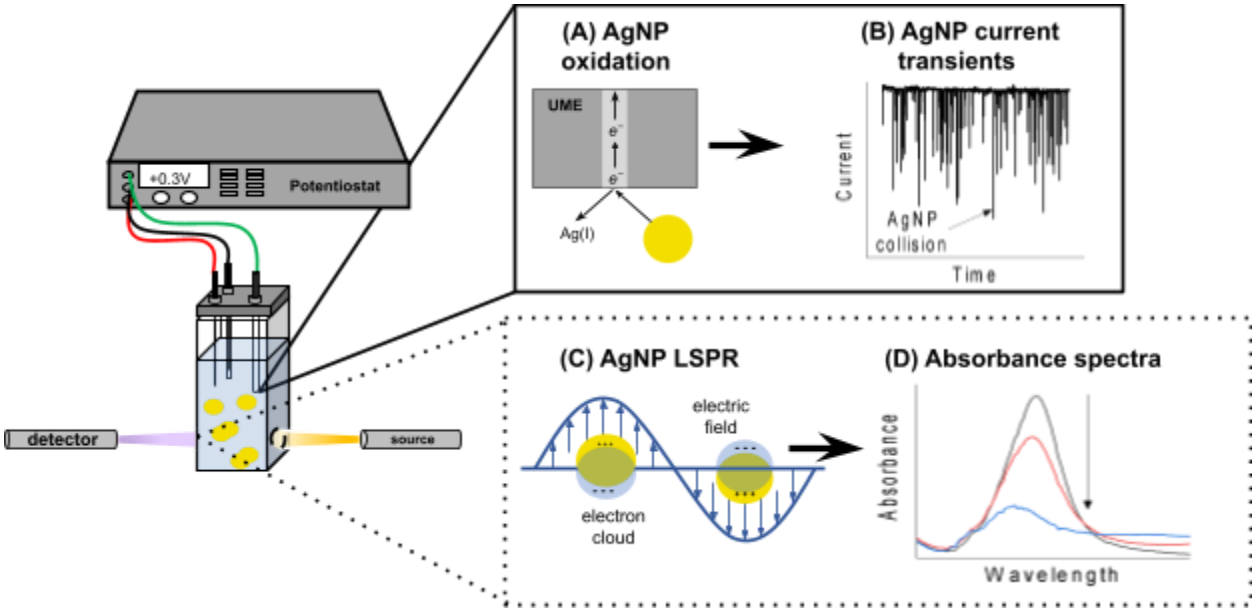

Figure 29. Particle impact voltammetry and UV-Vis schematic

With all of the experimental setup complete, measuring nanoparticle-protein binding could be accomplished via the schematic in Figure 29. For each concentration of protein, both a PIV measurement would be performed as well as a UV-Vis spectrogram. This could then be used to fit two langmuir isotherms and compare the binding constants using each technique.

Results and Discussion

Once the experimental setup was optimized and the method was fully designed, testing could begin to determine the feasibility of using this technique to measure nanoparticle-protein binding constants. The first step was to ensure that the addition of proteins into the sample matrix did not interfere with the electrode directly and was observed as a change in PIV signal frequency. The results shown in Figure 30 demonstrate that a difference in the number of transients is observed after the addition of a protein (HSA). However, these results were not consistently reproducible due to the sensitivity requirements of PIV and the small signal-to-noise ratio obtained (as is seen in Figure 30a).

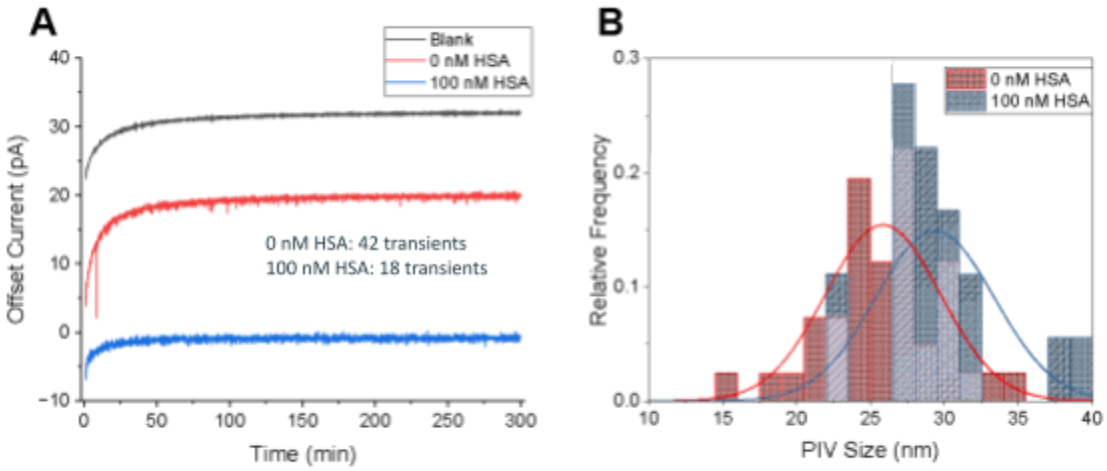

Figure 30. Change in PIV signal upon addition of 100 nM human serum albumin. Demonstrating both (A) the change in the number of transients and (B) the change in the size distribution of those particles.

One of the major flaws of this initial design was that the particle size chosen was small enough that the signals would often get captured inside the noise of the measurement. This invalidated the accuracy of any results obtained for most PIV runs. The way around this was to use larger particles. In Figure 31, it was shown that 60 nm AgNPs yield much more resolved data.

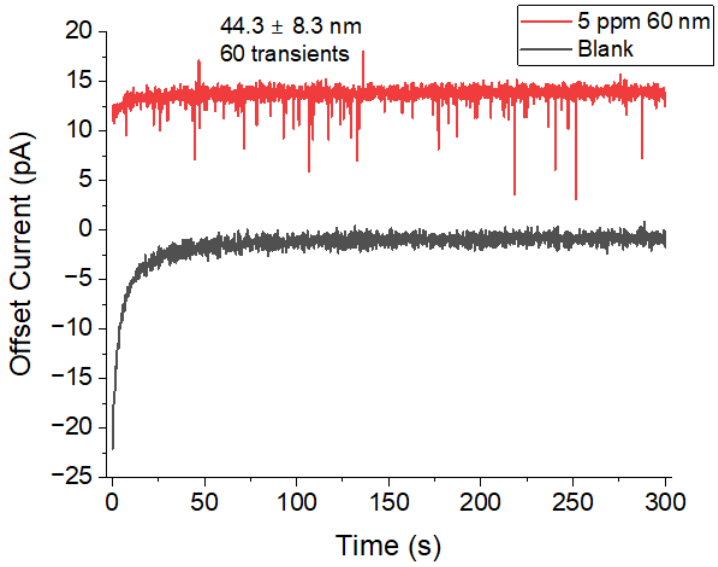

Figure 31. PIV measurement of 60 nm AgNPs, representing a signal that is no longer trapped in the background noise.

However, towards the end of this project, when the switch to using 60 nm particles was made, there was not enough time to fully optimize this technique. Thus, the interaction

between 60 nm AgNPs and proteins was not able to be measured via PIV. Ideally, further work could be done to improve this design to be more suitable for analyzing larger AgNPs and the binding would be measurable.

So, as this project currently sits, only the first requirement was able to be met as a difference in PIV signal was able to be measured upon the addition of proteins into the AgNP sample matrix. However, since this was not reproducible with a range of protein concentrations, both the second and third requirements were not met. These are all problems that could be fixed in further iterations of the designed measurement scheme.

Conclusion

From these two projects, the utility of electrochemistry as a highly diverse measurement device has been realized. As is true in many facets of analytical chemistry and chemical engineering, as a whole, there are two sides to a successfully designed measurement schematic. Although the choice of instrumentation is crucial to the type of measurement, sensitivity, and overall produced data, an understanding of the fundamental tunability and physical limitations of these techniques can lead to much more creative approaches to solving difficult problems. In these projects, the fundamental limitations encountered in the literature stem from the use of highly specific techniques that are really good at doing one or two types of nanomaterial measurements. The high sensitivity achieved using these techniques often leads to them being utilized almost unanimously while still failing to offer data that could be used to understand some of the more nuanced interactions between nanomaterials and their local environment.

As has been discussed at length, the use of electrochemistry has allowed for the design of multiple schematics that bridge the gap between different nanomaterial transformation measurements. In Project 1, the coupling of linear sweep stripping voltammetry (LSSV) and particle impact voltammetry (PIV) has allowed for the release mechanisms of both AgNPs and Ag(I) from nano-enabled textiles to be understood at kinetic resolutions, a result that has never been seen in the literature. Additionally, this technique has further pushed the

bounds of nanomaterial analysis by allowing for the size of these nanoparticles to be analyzed over time in tandem. Similarly, in Project 2, the interaction between these released nanoparticles and proteins in the environment is beginning to be understood via PIV. While this method still needs to undergo more optimization, the preliminary results gathered thus far are promising. Once complete, this measurement design will allow for an understanding of how biological molecules bind onto the surface of nanomaterials.

While nanomaterial research and material science, more generally, continue to evolve into new and up-and-coming industries, and as applications of these materials become more widespread, it is becoming increasingly important to understand their environmental impact. While current methods for analyzing these materials in their newly produced forms are sufficient for baseline characterizations before mass production, end-of-use analyses and techniques suitable for understanding the environmental effects of these materials are lagging behind. Therefore, designing methods for understanding these interactions is paramount for maintaining a proper balance between material innovation and environmental consciousness.

Summary of Design Specifications

Table 4. Design Specifications for Multifunctional Nanomaterial Analyses Using Inexpensive Techniques

Project 1: *Release Dynamics of AgNPs and Ag(I) from Embedded Textiles*	**Constraints**	1. The sensitivity of the instrument needed to be high enough to detect both the **transients of the nanoparticles** measured as well as the **current peaks of the silver ions** measured.	
		2. The instrument needs to **maintain this sensitivity over a four-hour measurement period**.	
		3. The **fabric utilized can not interfere with the measurement** or else the data obtained would not be reliable or reproducible.	
		4. Without the resources that are already in the lab, the project would cost approximately **$10,000** starting from the ground up.	
	Requirements	1. The method needs to allow for the **measurement of both AgNPs and Ag(I) concentrations** released from AgNP-enabled textiles.	✓ Both AgNPs and Ag(I) concentrations were able to be measured over time
		2. The method needed to allow for the **construction of time-dependent concentration plots** to understand the release kinetics of both AgNPs and Ag(I) over time as well as the **correlation between the release of the two species**.	✓ Kinetically resolved data was collected and revealed a unique correlation between AgNP and Ag(I) release
		3. The method must be **reproducible** across different sweat conditions, different fabrics, and over different days.	✓ This method was highly reproducable across different fabric samples and several different sweat conditions
Project 2: *Understanding Protein Interactions with AgNP*	**Constraints**	1. The sensitivity of the instrument needs to be high enough to **measure the transients of the nanoparticles measured**.	
		2. The **proteins added to the nanoparticles can not interfere** with the electrochemical measurement, or else the data obtained would not be reliable.	
		3. Without the resources that are already in the lab, the project would cost approximately **$10,000** starting from the ground up.	
	Requirements	1. The method needs to **allow for the detection of protein-nanoparticle interactions** via a change in PIV signal.	✓ The protein-nanoparticle interaction was detected as a difference in PIV signal
		2. The method needed to allow for the **determination of protein-nanoparticle binding constants via a change in PIV signal as a function of protein concentration**. This would then be fit using a Langmuir isotherm.	! The method was not optimized enough to measure a difference in PIV concentration as a function of protein concentration
		3. The method must **yield results similar to other techniques** previously utilized within a similar analysis time frame.	! Since no binding constant was measurable, there was nothing to compare to external results

Acknowledgments

I would like to thank both of my advisors for their support throughout this project. Professor Carr Everabach in the Engineering Department at Swarthmore was very helpful in keeping me on track and ensuring that my project passed the E90 qualifications. Professor Kathryn Riley in the Swarthmore Chemistry and Biochemistry Department has been the inspiration for this work and has continued to help me through every step of my Swarthmore process. I've been blessed with the opportunity to work in Professor Riley's lab for the past two years. I'd also like to thank all of my current and past labmates in the Riley lab. They helped to keep me sane when things weren't working well, which was not an uncommon occurrence. And to my mom, dad, my two brothers, and the rest of my wonderful family, I truly couldn't have gotten to this point without any of you. Thank you!

References

(1) Bryan Calderón-Jiménez; Monique E. Johnson; Antonio R. Montoro Bustos; Karen E. Murphy; Michael R. Winchester; José R. Vega Baudrit. Silver Nanoparticles: Technological Advances, Societal Impacts, and Metrological Challenges. *Frotiers Chem.* **2017**. https://doi.org/10.3389.

(2) Gorka, D. E.; Lin, N. J.; Pettibone, J. M.; Gorham, J. M. Chemical and Physical Transformations of Silver Nanomaterial Containing Textiles after Modeled Human Exposure. *NanoImpact* **2019**, *14*, 100160. https://doi.org/10.1016/j.impact.2019.100160.

(3) Hui, J.; O'Dell, Z. J.; Rao, A.; Riley, K. R. In Situ Quantification of Silver Nanoparticle Dissolution Kinetics in Simulated Sweat Using Linear Sweep Stripping Voltammetry. *Environ. Sci. Technol.* **2019**, *53* (22), 13117–13125. https://doi.org/10.1021/acs.est.9b04151.

(4) Quadros, M. E.; Pierson, R.; Tulve, N. S.; Willis, R.; Rogers, K.; Thomas, T. A.; Marr, L. C. Release of Silver from Nanotechnology-Based Consumer Products for Children. *Environ. Sci. Technol.* **2013**, *47* (15), 8894–8901. https://doi.org/10.1021/es4015844.

(5) Durán, N.; Silveira, C. P.; Durán, M.; Martinez, D. S. T. Silver Nanoparticle Protein Corona and Toxicity: A Mini-Review. *J. Nanobiotechnology* **2015**, *13* (1), 1–17.

(6) Mott, D.; Galkowski, J.; Wang, L.; Luo, J.; Zhong, C.-J. Synthesis of Size-Controlled and Shaped Copper Nanoparticles. *Langmuir* **2007**, *23* (10), 5740–5745. https://doi.org/10.1021/la0635092.

(7) Calahorra, Y.; Shtempluck, O.; Kotchetkov, V.; Yaish, Y. E. Young's Modulus, Residual Stress, and Crystal Orientation of Doubly Clamped Silicon Nanowire Beams. *Nano Lett.* **2015**, *15* (5), 2945–2950. https://doi.org/10.1021/nl5047939.

(8) Reddy, L. H.; Arias, J. L.; Nicolas, J.; Couvreur, P. Magnetic Nanoparticles: Design and Characterization, Toxicity and Biocompatibility, Pharmaceutical and Biomedical Applications. *Chem. Rev.* **2012**, *112* (11), 5818–5878. https://doi.org/10.1021/cr300068p.

(9) Haes, A. J.; Van Duyne, R. P. A Nanoscale Optical Biosensor: Sensitivity and Selectivity of an Approach Based on the Localized Surface Plasmon Resonance Spectroscopy of Triangular Silver Nanoparticles. *J. Am. Chem. Soc.* **2002**, *124* (35), 10596–10604. https://doi.org/10.1021/ja020393x.

(10) Huang, H.; Liu, R.; Yang, J.; Dai, J.; Fan, S.; Pi, J.; Wei, Y.; Guo, X. Gold Nanoparticles: Construction for Drug Delivery and Application in Cancer Immunotherapy. *Pharmaceutics* **2023**, *15* (7), 1868. https://doi.org/10.3390/pharmaceutics15071868.

(11) Jin, W.; Deng, Y.; Guo, B.; Lian, Y.; Zhao, B.; Di, D.; Sun, X.; Wang, K.; Chen, S.; Yang, Y.; Cao, W.; Chen, S.; Ji, W.; Yang, X.; Gao, Y.; Wang, S.; Shen, H.; Zhao, J.; Qian, L.; Li, F.; Jin, Y. On the Accurate Characterization of Quantum-Dot Light-Emitting Diodes for Display Applications. *Npj Flex. Electron.* **2022**, *6* (1), 1–12. https://doi.org/10.1038/s41528-022-00169-5.

(12) Wang, L.; Teles, M. P. R.; Arabkoohsar, A.; Yu, H.; Ismail, K. A. R.; Mahian, O.; Wongwises, S. A Holistic and State-of-the-Art Review of Nanotechnology in Solar Cells. *Sustain. Energy Technol. Assess.* **2022**, *54*, 102864. https://doi.org/10.1016/j.seta.2022.102864.

(13) Smijs, T. G.; Pavel, S. Titanium Dioxide and Zinc Oxide Nanoparticles in Sunscreens:

Focus on Their Safety and Effectiveness. *Nanotechnol. Sci. Appl.* **2011**, *4*, 95–112. https://doi.org/10.2147/NSA.S19419.
(14) Loos, M. Chapter 1 - Nanoscience and Nanotechnology. In *Carbon Nanotube Reinforced Composites*; Loos, M., Ed.; William Andrew Publishing: Oxford, 2015; pp 1–36. https://doi.org/10.1016/B978-1-4557-3195-4.00001-1.
(15) Mayer, K. M.; Hafner, J. H. Localized Surface Plasmon Resonance Sensors. *Chem. Rev.* **2011**, *111* (6), 3828–3857. https://doi.org/10.1021/cr100313v.
(16) Mishra, N.; Liu, M.; Fang, Y.; Kulkarni, S. Study of Adsorption Behavior of Aminothiophenols on Gold Nanorods Using Surface-Enhanced Raman Spectroscopy. *J. Nanophotonics* **2011**, *5*, 053513. https://doi.org/10.1117/1.3594096.
(17) Monaghan, J. W.; O'Dell, Z. J.; Sridhar, S.; Paranzino, B.; Sundaresan, V.; Willets, K. A. Calcite-Assisted Localization and Kinetics (CLocK) Microscopy. *J. Phys. Chem. Lett.* **2022**, *13* (45), 10527–10533. https://doi.org/10.1021/acs.jpclett.2c03028.
(18) Pourzahedi, L.; Vance, M.; Eckelman, M. J. Life Cycle Assessment and Release Studies for 15 Nanosilver-Enabled Consumer Products: Investigating Hotspots and Patterns of Contribution. *Environ. Sci. Technol.* **2017**, *51* (12), 7148–7158. https://doi.org/10.1021/acs.est.6b05923.
(19) Köser, J.; Engelke, M.; Hoppe, M.; Nogowski, A.; Filser, J.; Thöming, J. Predictability of Silver Nanoparticle Speciation and Toxicity in Ecotoxicological Media. *Environ. Sci. Nano* **2017**, *4* (7), 1470–1483. https://doi.org/10.1039/C7EN00026J.
(20) Kulthong, K.; Srisung, S.; Boonpavanitchakul, K.; Kangwansupamonkon, W.; Maniratanachote, R. Determination of Silver Nanoparticle Release from Antibacterial Fabrics into Artificial Sweat. *Part. Fibre Toxicol.* **2010**, *7* (1), 8. https://doi.org/10.1186/1743-8977-7-8.
(21) Hedberg, J.; Skoglund, S.; Karlsson, M.-E.; Wold, S.; Odnevall Wallinder, I.; Hedberg, Y. Sequential Studies of Silver Released from Silver Nanoparticles in Aqueous Media Simulating Sweat, Laundry Detergent Solutions and Surface Water. *Environ. Sci. Technol.* **2014**, *48* (13), 7314–7322. https://doi.org/10.1021/es500234y.
(22) Rice, S. B.; Chan, C.; Brown, S. C.; Eschbach, P.; Han, L.; Ensor, D. S.; Stefaniak, A. B.; Bonevich, J.; Vladár, A. E.; Walker, A. R. H.; Zheng, J.; Starnes, C.; Stromberg, A.; Ye, J.; Grulke, E. A. Particle Size Distributions by Transmission Electron Microscopy: An Interlaboratory Comparison Case Study. *Metrologia* **2013**, *50* (6), 663–678. https://doi.org/10.1088/0026-1394/50/6/663.
(23) Holbrook, R. D.; Rykaczewski, K.; Staymates, M. E. Dynamics of Silver Nanoparticle Release from Wound Dressings Revealed via in Situ Nanoscale Imaging. *J. Mater. Sci. Mater. Med.* **2014**, *25* (11), 2481–2489. https://doi.org/10.1007/s10856-014-5265-6.
(24) Ellison, J.; Tschulik, K.; Stuart, E. J. E.; Jurkschat, K.; Omanović, D.; Uhlemann, M.; Crossley, A.; Compton, R. G. Get More Out of Your Data: A New Approach to Agglomeration and Aggregation Studies Using Nanoparticle Impact Experiments. *ChemistryOpen* **2013**, *2* (2), 69–75. https://doi.org/10.1002/open.201300005.
(25) Rees, N. V.; Zhou, Y.-G.; Compton, R. G. Making Contact: Charge Transfer during Particle–Electrode Collisions. *RSC Adv* **2012**, *2* (2), 379–384. https://doi.org/10.1039/C2RA01100J.
(26) Perera, Y. R.; Hill, R. A.; Fitzkee, N. C. Protein Interactions with Nanoparticle Surfaces: Highlighting Solution NMR Techniques. *Isr. J. Chem.* **2019**, *59* (11–12), 962–979. https://doi.org/10.1002/ijch.201900080.

(27) Allen J. Bard; Larry F. Faulkner. Electrochemical Methods, Fundamentals and Applications. 2nd Ed. John Wiley & Sons; New York, NY, USA: 2001.
(28) Florence, T. M. Determination of Trace Metals in Marine Samples by Anodic Stripping Voltammetry. *J. Electroanal. Chem. Interfacial Electrochem.* **1972**, *35* (1), 237–245. https://doi.org/10.1016/S0022-0728(72)80311-5.
(29) Cheng, W.; Compton, R. G. Electrochemical Detection of Nanoparticles by 'Nano-Impact' Methods. *New Nanobiosensing Tech. Bioanal.* **2014**, *58*, 79–89. https://doi.org/10.1016/j.trac.2014.01.008.
(30) Heyrovsky, M.; Jirkovsky, J. Polarography and Voltammetry of Ultrasmall Colloids: Introduction to a New Field. *Langmuir* **1995**, *11* (11), 4288–4292. https://doi.org/10.1021/la00011a020.
(31) Xiao, X.; Bard, A. J. Observing Single Nanoparticle Collisions at an Ultramicroelectrode by Electrocatalytic Amplification. *J. Am. Chem. Soc.* **2007**, *129* (31), 9610–9612. https://doi.org/10.1021/ja072344w.
(32) Jiang, J.; Huang, X.; Wang, L. Effect of Forced Convection on the Collision and Interaction between Nanoparticles and Ultramicroelectrode. *J. Colloid Interface Sci.* **2016**, *467*, 158–164. https://doi.org/10.1016/j.jcis.2016.01.009.

Appendix

Appendix A: Calculation of Zeta Potential

Determine electrophoretic mobility (μ_e) two ways

$$\mu_e = \frac{V}{E}$$

where V = particle velocity (μm/s), E = electric field strength (V/cm)

$$\mu_e = \frac{2\varepsilon_r \cdot \varepsilon_0 \cdot \zeta \cdot f(Ka)}{3\eta},$$

where ε_r = relative permittivity/dielectric constant, ε_0 = permittivity of vacuum, ζ = Zeta Potential, f(Ka) = Henry's function , η = viscosity

When the electric double layer (thickness of two oppositely charged ions on the surface of the particle) is large compared to the particle radius (i.e., for particles < 100 nm or in low salt conditions), f(Ka) can be approximated by 1. Thus yielding:

$$\mu_e = \frac{2\varepsilon_r \cdot \varepsilon_0 \cdot \zeta}{3\eta}$$

Solving for the Zeta potential

$$\zeta = \frac{3\eta \cdot V}{2\varepsilon_r \cdot \varepsilon_0 \cdot E}$$

Appendix B: Calculation/dimensional analysis of particle diameter based on PIV data

$$V = \frac{4}{3}\pi r^3$$

$$V\,[=]\,cm^3$$

$$A_r\,[=]\,\frac{g}{mol},\ N_a\,[=]\,\frac{molecules}{mol},\ N\,[=]\,molecules,\ \rho\,[=]\,\frac{g}{cm^3}$$

$$\frac{A_r \cdot N}{N_a \cdot \rho}\,[=]\,\frac{\frac{g}{mol} \cdot molecules}{\frac{molecules}{mol} \cdot \frac{g}{cm^3}} = cm^3$$

$$V = \frac{A_r \cdot N}{N_a \cdot \rho} = \frac{4}{3}\pi r^3 = \frac{4}{3}\pi\left(\frac{d}{2}\right)^3$$

$$d = 2 \cdot \sqrt[3]{\frac{3 \cdot A_r \cdot N}{4\pi \cdot N_a \cdot \rho}}$$

Appendix C. Macro command for the four-hour fabric release experiments

```
for: 36

tech: lsv
smodeon
depe: -0.5
dept: 60
ei: -0.5
eh: 0.6
v: 0.05
qt: 5       # Quiet Time
si: 0.005
sens: 1e-9
run
save: 070723_FabricRelease1_LSSV

tech: i-t
ei: 0.6
si: 0.1
st: 300
qt: 2
sens: 1e-10
run
save: 070723_FabricRelease1_PIV

tech: lsv
smodeoff
ei: 0.6
eh: -0.5
v: 0.3
qt: 0       # Quiet Time
si: 0.005
sens: 1e-8
run
next
```